# Functional model for analysis of ALD nucleation and quantification of area-selective deposition

Gregory N. Parsons

Citation: Journal of Vacuum Science & Technology A 37, 020911 (2019); doi: 10.1116/1.5054285

View online: https://doi.org/10.1116/1.5054285

View Table of Contents: https://avs.scitation.org/toc/jva/37/2

Published by the American Vacuum Society



## Functional model for analysis of ALD nucleation and quantification of area-selective deposition

Gregory N. Parsons

Department of Chemical and Biomolecular Engineering, North Carolina State University, Raleigh, North Carolina 27695

(Received 30 August 2018; accepted 21 December 2018; published 23 January 2019)

Bottom-up chemical patterning, to additively form material only in desired locations, is becoming important to address scaling issues in semiconductor device manufacturing, catalytic material design, and other fields utilizing nanometer- and sub-nanometer-scaled material features. In some semiconductor device fabrication steps, chemically driven patterning by area-selective deposition (ASD) is beginning to supplant physical patterning by photolithography. To advance the field of ASD, more understanding is needed regarding mechanisms of thin film nucleation, particularly when nucleation proceeds where thin film deposition is not desired. To better understand thin film nucleation, this work describes a relatively simple analytical model with three adjustable input parameters that quantifies film growth initiation, island growth, and thickness evolution during area-selective atomic layer deposition (AS-ALD) and area-selective chemical vapor deposition. A definition is presented for chemical selectivity during film growth that depends on the extent of film coverage in the desired non-growth region. Fitting the model with experimental data gives quantitative output that allows the extent of selectivity to be compared for different ASD approaches studied in different labs, with data collected using a variety of analytical tools. Using several example published AS-ALD data sets, the article demonstrates how fitting the model to experimental data gives insight into different nucleation mechanisms for unwanted film growth during ASD. The author further describes how the model can be improved and expanded to encompass more complex film growth and nucleation mechanisms. Published by the AVS. https://doi.org/10.1116/1.5054285

#### I. INTRODUCTION

#### A. Background

An overarching challenge in the field of thin film deposition is to better understand fundamental mechanisms during nucleation and growth initiation. In general, any chemical deposition reaction, such as atomic layer deposition (ALD) or chemical vapor deposition (CVD), will be influenced by the chemical and physical nature of the surface that is being covered by the deposit. The deposition substrate can have a strong impact on how the growth reactions begin, and how the film evolves after nucleation. Several types of "substratedependent" or "substrate-selective" deposition can be identified, 1,2 including shape- or direction-selective deposition, where deposition on one surface proceeds in a desired direction, with different growth on another surface; structure-selective deposition, where, for example, a crystalline film grows on one surface, with a different structure (e.g., amorphous) on another surface; composition-selective deposition, producing films with different chemical composition in different locations; and area-selective deposition (ASD), leading to uniform deposition in a desired "growth" region and no deposition in desired "non-growth" regions.<sup>2–</sup>

While nucleation mechanisms are important in any substrate-dependent deposition process, this article addresses means to understand and analyze nucleation specifically for area-selective deposition. The expanding demand for low

Note: This paper is part of the 2019 special collection on Atomic Layer Deposition (ALD).

temperature area-selective deposition, particularly for sub-10 nm semiconductor device patterning,<sup>5</sup> is encouraging more researchers to study surface-dependent processes in atomic layer deposition, chemical vapor deposition, and atomic layer etching. An example application for ASD is the "fully aligned via," shown schematically in Fig. 1. In semiconductor device manufacturing, lithographic patterning is used to open via holes to connect metal lines through an insulating layer. Any misalignment between the via and the underlying target metal results in "edge placement error" (EPE), which can lead to shorting between the via metal and neighboring metal line. As device dimensions shrink, cost-effective lithography is not able to maintain the EPE required for high yield. To overcome this problem, manufacturers seek an ASD solution to create a physical barrier between the metal lines, thereby minimizing the risk of EPE-related shorting.

Implementing area-selective deposition in device fabrication represents an important transition in manufacturing science. Specifically, top-down physical alignment by lithography, which has been dominant since the earliest days of semiconductors, is being usurped by "bottom-up" or "self-aligned" chemical patterning. In bottom-up patterning, material is formed additively only in desired locations. For device fabrication, the desired patterns are generally determined by previous processing steps, so that the as-prepared surface presents multiple materials with different chemical properties. In ASD, the required precision in material placement is met by taking advantage of these differences in atomic-scale chemical information present on the surface being coated, rather than utilizing physical information present in a photomask. In

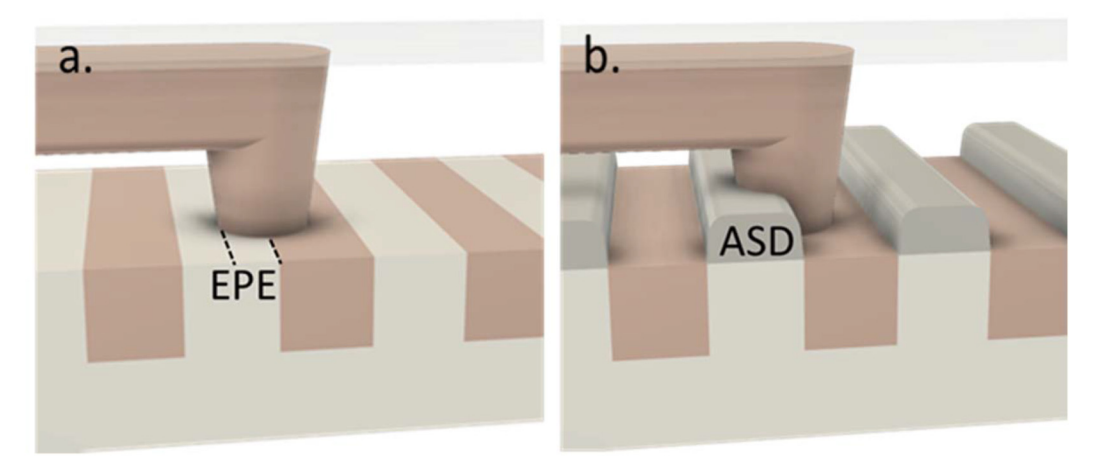


Fig. 1. Schematic illustration of dual-damascene back-end metalization with the interlayer dielectric layer removed for visualization: (a) a misaligned via hole resulting in edge placement error (EPE) for the metalized via relative to the substrate metal line, creating a potential electrical short or electromigration path between the via metal and the neighboring substrate metal line and (b) a misaligned via hole after area-selective deposition (ASD) of dielectric on the dielectric spacer lines between substrate metal lines, creating a physical barrier to avoid electrical shorting to the neighboring substrate metal line.

some cases where patterns are not previously defined, additional steps are used to define the desired growth pattern. To achieve reliable ASD, new tools are needed to access and quantify chemical information on patterned substrates.

From basic thermodynamics, we understand that deposition reactions with ALD precursors and coreactants will strongly depend on the surface composition and surface termination, so that some surfaces will be strongly receptive to growth while others will be relatively inert. At elevated temperatures (>700 °C) differences in surface/adspecies adsorption equilibria can be very large, allowing substrate-selective epitaxy to be sufficiently controlled for large-scale manufacturing. However, many device fabrication steps require much lower processing temperatures (<400 °C) where surface passivation layers (e.g., Si-H and Si-OH on silicon and silicon dioxide) modulate surface energy, making thermodynamic differences in reactivity less pronounced. Some surfaces have a large density of chemical sites that will react readily with ALD reactants allowing layer-by-layer growth from the first ALD cycles. On the other hand, surfaces can contain few or even no measureable reactant sites. These surfaces show inhibited growth, but inevitably, extended deposition leads to visible nuclei "islands" that coalesce into a continuous film. This "island growth" on less-receptive surfaces is widely observed and modeled by several researchers. 6-8

To address the challenge of understanding film nucleation, we use island growth modeling to characterize mechanisms in growth initiation and film nucleation on surfaces that are either naturally nonreceptive or designed to be nonreceptive to ALD. Further, using previously described definitions of chemical selectivity during film growth, we show how island growth modeling can be used to quantitatively compare ASD results from different materials, processes, and experimental laboratories.

#### B. Approaches to ASD

There are many approaches reported to achieve ASD of metals and dielectric materials by ALD or CVD on patterned surfaces. Researchers often categorize the different approaches as "inherent," "activated," and "passivated" selective deposition. "Inherent" selectivity generally occurs on a clean or otherwise unmodified patterned surface. In this case, slow nucleation during ALD or CVD on one surface allows desired material to form on the faster nucleating "growth" surface, before substantial nucleation occurs on the slower nucleating "non-growth" surface. Inherent selectivity has yielded satisfactory results in a few material systems. "Activated" selectivity can proceed using a patterned flux from an external energy source (e.g., photons, electrons, ions, etc.) impinging on a surface to yield growth predominantly in the energized areas. Activated selectivity can also occur when one region of a surface locally catalyzes reactant activation, producing selective growth. Activated processes are generally difficult to scale, and they work for only limited materials. "Passivated" selectivity proceeds by introducing before deposition an additional chemical species that is not a deposition reactant that adsorbs and/or binds to only one of the exposed regions on the clean unmodified starting surface. This passivating agent or "blocking layer" acts to impede reactant adsorption in the coated region. The passivating material is then removed after ASD. A wide range of blocking materials can be used, and the passivated ASD approach can be scaled, but the addition and removal of the passivating agent adds material burden in the process and new complexity in the process optimization.

Inherent, activated, and passivated ASD can be done using common binary or "two-step" A/B ALD reactions. Inevitably, extended deposition yields unwanted growth and/or surface contamination, which eliminates the desired chemical differences between the growth and non-growth surface. Recently, new "three-step" methods have appeared where an extra step or sequence is added into the two-step ALD cycle. The extra step is generally designed to clean or otherwise renew the non-growth surface, thereby improving chemical differentiation between the growth and non-growth regions. 9-11 "Three-step" ASD can include, for example, A/B/C ALD

sequences that dose a surface adsorbing compound in each cycle to refresh the surface passivation. Another version of a "three-step" method involves using integrated ALD+etch supercycles, where a short etch step or sequence is used after several ALD cycles to remove undesired nuclei. The dep/etch supercycles can be repeated multiple times to grow up the desired film thickness. Many of the three-step processes are intriguing, but they introduce additional complexity and new issues regarding material and reactant interactions.

### C. Previous models for inhibited or island growth during ALD

In area selective deposition, inhibited nucleation in the nongrowth region produces islands that grow and coalesce. Several empirical models have been developed to describe the trends observed during inhibited growth. Alam and Green<sup>6</sup> developed kinetic expressions for nucleation and growth during ALD of HfO2 from HfCl4 and water on receptive Si-OH and inhibited Si-H surfaces. The model included analysis of the film deposition reaction rate on pre-existing and generated nucleation sites (i.e., -OH on Si-H surfaces). Consistent with experiments, the model indicated that initial growth on inhibited surfaces follows a parabolic trend, including an apparent accelerated deposition rate at intermediate surface coverage. In this model, the accelerated rate resulted from an excess of surface –OH sites on isolated nuclei or nuclei edges relative to that on the flat growth surface. The model did not analyze or predict how surface coverage fraction on inhibited surfaces would evolve as ALD proceeds. Puurunen et al. and Nilsen et al.8 further developed island growth models to understand and analyze trends in film growth on inhibited surfaces, including predictions for surface coverage fraction. To allow geometric analysis of surface coverage, both of these studies assumed a starting density of growth sites arranged in a regular pattern on the starting surface. The models did not include possible effects of additional nucleation site generation during deposition, but did show apparent accelerated growth before nuclei coalescence, consistent with experimental trends. This is expected because on an isolated hemispherical nucleus, the total area receptive to growth is larger than the flat area of the substrate that the nucleus covers. However, because the models used a fixed density of nucleation sites arranged in a geometric (nonrandom) pattern, the predicted trends in thickness and growth rate gave nonphysical output that needed to be considered.

When analyzing any area-selective process, three key questions arise: First, how much material can be deposited in the desired growth region before substantial unwanted deposition appears in the non-growth region? Second, how does the effectiveness and quality of a given ASD process quantitatively compare to other ASD processes? And third, what mechanisms can account for undesired growth and other detrimental outcomes, and what can we do to improve overall process performance? This article describes a simple and usable empirical model, built using kinetic definitions of chemical selectivity and the well-known Avrami method of nucleation analysis, to show how fitting experimental ASD process data to the model

can help address these key questions. The model output provides values for deposition selectivity fraction, S, defined to range between 0 (i.e., equal growth rate on all surfaces) and 1 (i.e., zero growth rate on one surface with good growth on another), as well as values for one or more "selectivity demarcation parameters" or "figures of merit." We apply the model to published area-selective atomic layer deposition data and show how values of selectivity and demarcation parameters derived from model fits allow quantitative comparison of ASD results for different materials and methods obtained from different lab groups. We further demonstrate that the model fits give helpful insight into mechanisms responsible for unwanted film nucleation in different ASD processes.

### II. NUCLEATION DURING ALD, AND DEFINITION OF SELECTIVITY

#### A. Growth initiation and film nucleation

Surfaces that are receptive to growth often have a high density of surface termination sites (i.e., surface hydroxyls) that are reactive with the ALD precursor or coreactant. If the density of reactive sites on the starting surface is only slightly smaller than that on the growing film, the first few reactant dose steps show a smaller growth per cycle than measured later in the process. The effect can be small enough that it is not easily detected from a plot of thickness versus number of cycles.

A starting ALD surface can also be prepared with a very small density of reactive surface sites that are not easily detected experimentally. In some cases, the starting surface could be sufficiently prepared to have no available reactive sites. In these cases, experiments show that the amount of material deposited per cycle is very small (even zero) during the first ALD cycles, and continued ALD leads to observable nuclei, initially in the form of islands. Depending on the substrate composition, and crystallinity of the deposited film, the island nuclei can take on various shapes. High surface energy noble metals, for example, often form as spheres, and other metals form as faceted nanocrystals that depend on the substrate.

Once growth of a film begins under typical ALD conditions, the ALD sequence will lead to growth both laterally and upward at a constant rate determined by the ALD growth per cycle. Fixed nuclei will eventually join together to form a continuous film. Even for amorphous films, mechanisms including reactant surface diffusion and enhanced growth at nuclei edges could produce nonspherical nuclei. While the model discussed here specifically addresses formation and growth of spherical nuclei, the model could be adapted to include effects of nonspherical nuclei by implementing a mathematical description of the nonspherical nucleation and growth.

A key outstanding question in ALD is the identity and chemical nature of the surface sites where the first deposition reaction proceeds. The question is particularly interesting for the case of area-selective deposition, where we wish to impede growth on some exposed areas for as long as possible. The precise nature of the starting growth sites will of course depend on the substrate and precursors used for deposition. However, sites where growth begins generally fit into three categories: (1)

unwanted reactive sites present on the starting surface, such as hydroxyls, contamination, etc.; (2) sites generated during deposition by reactant or by-product species adsorbed on an otherwise pristine defect-free surface, where the species remain behind after the reactant purge step; and/or (3) sites otherwise generated during the ALD process, such as degradation or chemical conversion of surface passivating species.

Unwanted growth could begin on defect sites or on surfaces where defects are not initially present. Discussion on this topic can be confusing because researchers often identify unwanted nuclei as "defects," and the mechanisms leading to unwanted nuclei can be referred to as "defectivity," even though the starting surface could in principle be defect-free.

### B. Site generation during ALD, pattern-dependence, and surface loading effects

One possible mechanism for site generation during ALD could involve precursor adsorption and ligand exchange on the desired deposited film. Subsequent transport of the modified species by-product could create a growth site on an adjacent non-growth region. This mechanism has been proposed, for example, in area-selective CVD and ALD of tungsten. 15,16 This type of site generation would occur only after some desired film is deposited. This is an example of patterndependent selectivity, sometimes called "loading effects," where unwanted film tends to appear first near desired feature edges. "Loading effects" are known in plasma etching, where the etching can depend on the number of wafers loaded into the reactor. 17 In ASD, a large surface "loading" means a large fraction of the patterned surface is designed for desired growth. Loading can also vary across a wafer. For example, high local loading occurs near an isolated set of tightly clustered features.

In addition to unwanted adsorption of active by-products, other mechanisms could generate nucleation sites on an otherwise pristine defect-free surface. For example, if a precursor or precursor ligand has an affinity for physisorption on a non-growth surface, some small amount of that molecule may remain on the surface after the purge step. This remnant reactant could then promote ALD during the following coreactant dose, thereby creating a site for further growth.

### C. Feature overgrowth and other effects during ASD

For an ASD process, it is usually desirable for the ASD film to conform to the patterned substrate dimension. The cartoon in Fig. 1, for example, shows an ASD film with a width that matches the width of the underlying dielectric template. However, ALD generally produces film growth uniformly in all directions. Therefore, ASD processes often result in feature overgrowth, where the lateral dimension of the ASD layer exceeds that of the substrate. When ASD proceeds at the bottom of a via, for example, growth can emerge from the via to create a "mushroom" shape that is usually detrimental to the desired outcome. Other unwanted phenomena, such as wafer-scale nonuniformity, can also be observed in ASD processes. The model and related discussion presented here do not directly address these issues. However, the model as presented

can give insight into mechanisms that lead to these phenomena. Also, we believe the model could be readily extended to predict the expected shape and extent of feature overgrowth versus ASD conditions. Comparing experimental results to model analysis would help identify improved processes that minimize or otherwise modulate undesired ASD overgrowth or feature-dependent effects.

We also note that while surface species diffusion may be active during island growth, uniform ALD growth does not specifically quantify adspecies surface diffusion. Species diffusivity or diffusion rates do not appear as parameters in the model, and in the current model form, we believe useful quantitative output can be obtained without specifying adspecies diffusion processes. Adspecies diffusion may be important, for example, when critical nucleus size exceeds one atom, or during ASD overgrowth. While the uniform ALD growth mode used here specifies stationary nuclei, the overall nucleation model formalism could be amended to include other growth modes, including nuclei particle diffusion and agglomeration, such as that identified under some conditions during Pt ALD. <sup>12</sup>

#### D. Definition of chemical selectivity

The concept of chemical selectivity is well developed in the fields of chemical catalysis and reaction engineering, where reactions often lead to more than one product. Be Depending on the field and application, different definitions of selectivity are used. Overall selectivity is often defined as the ratio of the amount of desired product relative to the amount of undesired product. Also, the instantaneous or point selectivity refers to the relative formation rates of desired and undesired products. Desirable selectivity values are as large as possible. Perfect selectivity =  $\infty$ , and selectivity of 1 means that the process forms equal amounts of desired and undesired products.

For some systems, overall reactant utilization or total reaction output is important or convenient to measure. In this case, selectivity is defined as the amount (or rate) of one product relative to the total amount (or rate) of all products formed (or equivalently, the total amount or rate of reactant consumed). With this definition, perfect selectivity = 1 (i.e., all consumed reactant is converted into the desired product). When more than one product is formed, one can identify the selectivity of a particular product. For example, the "selectivity of product A" refers to the rate of formation of product A relative to the rate of reactant consumption, or equivalently, the fraction of reactant fed into the reactor that gets successfully converted into A. If two products are produced in equal amount, the selectivity of each product is then =  $\frac{1}{2}$ . Selectivity values on the two scales are related to each other. Writing  $S_1$ and  $S_{\infty}$  as the selectivity values on the 0-1 and 0- $\infty$  scales, respectively, then  $S_{\infty} = S_1/(1 - S_1)$ .

### E. Definition and analysis of selectivity during thin film deposition

The problem of defining and quantifying area-selectivity in thin film deposition has been approached in CVD.<sup>2-4</sup> Even

though deposition reactions proceed away from chemical equilibrium, the most basic definitions are based on reaction thermodynamics, where selectivity is the difference between overall reaction energy for deposition on the desired substrate and that on the undesired growth substrate.<sup>3</sup> This definition is not often practical for low temperature processes because the specific reactions that lead to undesired growth are not usually known.

Unlike the chemical processes discussed above that produce more than one product, area-selective deposition involves only one product which is desired in one location but not in another. Considering this, the definitions for selectivity described above can be adapted to define selectivity for area-selective deposition, which will be evaluated as a function of the extent of deposition in the desired growth region. Creighton<sup>15</sup> noted that when few nucleation sites are produced, the surface coverage after a period of time will be proportional to the starting nuclei density. Gladfelter<sup>4</sup> expanded on this to quantify selectivity for area-selective CVD. He argued that the thermodynamic definition could be approximated by a chemical kinetic definition, where for apparent first-order nucleation, selectivity on a given surface,  $S_1$ , is given by the rate of nucleation on that surface relative to the total nucleation rate on all exposed growth surfaces. For two surfaces, this leads to  $S_1 = [k_1/(k_1 + k_2)]$ . However, directly measuring nucleation rate is difficult. Fortunately, during initial film growth, the nucleation rate is directly related to the number of nuclei on the surface, which can be obtained from the measured fraction of the substrate covered by the nuclei,  $\theta_1$ , relative to that on an adjacent surface,  $\theta_2$ . Analogous to the definition given above for product selectivity in chemical processing, the deposition selectivity on a given surface,  $S_1$ , can be defined as  $S_1 = [\theta_1/(\theta_1 + \theta_2)]$ . The overall selectivity, S, can then be defined as the difference between the selectivity on surface 1 (i.e., the desired growth surface) and the selectivity on surface 2 (i.e., the desired non-growth surface)

$$S = \frac{\theta_1}{\theta_1 + \theta_2} - \frac{\theta_2}{\theta_1 + \theta_2} = \frac{\theta_1 - \theta_2}{\theta_1 + \theta_2}.$$
 (1)

It is important to note that this definition is related to the more formal kinetic definition only under limited conditions (i.e., low surface coverage, no nuclei coalescence, first-order nucleation rate). Recognizing this formal limitation, Eq. (1) can be extended outside the formal limit and used as a general empirical definition of selectivity in film deposition. This definition follows the same formalism, for example, as that used to define enantiomeric excess in racemic mixtures.

Examining Eq. (1), we see that the value for S will range from S=1 (perfect selectivity, i.e.,  $\theta_2=0$ ) to S=0 (nonselective, i.e.,  $\theta_1=\theta_2$ ). This allows the extent of selectivity after any deposition process to be reported as fractional percentage. For example, if a process gives full coverage on the desired growth surface with 5% coverage on the "nongrowth" surface, then  $S=(1-0.05)/(1+0.05)\approx 0.905$ . Also, like the definitions of selectivity identified above, this value of S on a 0-1 scale can be converted to a  $0-\infty$  scale using  $S_\infty = S_1/(1-S_1)$ . The rate of nucleation on the non-growth

surface will depend on growth time during CVD and on the number of cycles in ALD. This means that as growth continues, additional coverage on the non-growth surface will reduce the value of S as a function of time or cycles.

To determine the selectivity obtained by ASD process, the  $\theta$  values to be input into Eq. (1) can be measured directly, for example, by scanning electron microscopy or AFM, or inferred from film thickness or other methods. To use film thickness, we note that for hemispherical or otherwise nonplanar nuclei, the planar surface area covered by the nuclei, i.e., the values for  $\theta$  in Eq. (1), are directly related to the total deposited film volume, deposited atomic density, or average distributed film thickness, which can be estimated, for example, using spectroscopic ellipsometry, Auger electron spectroscopy, XPS, SEM, Rutherford backscattering, or other techniques. To determine values of  $\theta$  using XPS or AES, data will need to be adjusted to include effects of the escape depth of the detected electrons. This is discussed below in relation to Eq. (17) and data in Fig. 7.

The definition of area-selectivity in film deposition in Eq. (1) avoids problems with other empirical definitions. For example, if selectivity is defined by material deposited before a nucleation induction time or ALD induction cycle number (i.e., when unwanted material starts to be observed on the non-growth surface), then the degree of selectivity will depend on the tool used to detect unwanted growth. For some applications where very high selectivity is required, knowledge of "undetected" nuclei can be critical.

To approach the problem of selectivity analysis, a means is needed to use experimental data (usually film deposition thickness) to estimate surface coverage fraction as a function of deposition time or number of ALD cycles. As shown below, a simple analytical model allows the trend in thickness on the non-growth surface versus ALD cycle to be correlated with surface coverage fraction. Then, by collecting several data points for the extent of unwanted film growth versus time (or ALD cycles) and fitting the trend to the model, the selectivity fraction defined in Eq. (1) can be determined as a function of the amount of film deposited in the desired growth region. The model below can be used with data collected by many different techniques to produce a quantitative value of selectivity that can be compared between different data sets collected in different laboratories. The model uses four independent parameters: (i) the ALD growth thickness per cycle at steady state,  $\dot{G}$  (nm/cycle) (i.e., the thickness per cycle when a material deposits on itself); (ii) the number of nucleating sites present per unit area in the starting non-growth region,  $\hat{N}$  (nm<sup>-2</sup>); (iii) the number of nucleating sites generated per cycle per unit area in the non-growth region,  $\dot{N}_0$  (nm<sup>-2</sup> cycle<sup>-1</sup>); and (iv) the characteristic number of ALD cycles for delay in nucleation site generation,  $v_d$  (cycle). These and other terms are summarized in Table I and defined in more detail below.

### III. AVRAMI MODEL FOR ALD FILM NUCLEATION AND ISLAND GROWTH

We set out to identify a phenomenological model to describe trends commonly observed in substrate-inhibited ALD, and define means to use the model to quantitatively analyze

TABLE I. Parameters used in the analytical model calculation.

Parameter	Units	Description			
S	_	Deposition selectivity, defined as a fraction			
		between 0 and 1			
$A_f$	$nm^2$	Area of the substrate covered by film			
$A_0$	$nm^2$	Area of the substrate			
n	cycles	Number of ALD cycles (or CVD time)			
$\dot{G}$	nm cycle <sup>-1</sup>	Growth rate for a material depositing on itself			
$\hat{N}$	$nm^{-2}$	Nucleation site density on starting non-growth			
		surface			
$\dot{N}_0$	nm <sup>-2</sup> cycle <sup>-1</sup>	Nucleation site generation rate on non-growth			
		surface			
$\nu_d$	cycles	Nucleation site generation delay cycles on			
		non-growth surface			
$\tilde{t}_{ng}$	nm	Approximate calculated film thickness in			
-		non-growth region			
$t_{ng}$	nm	Calculated film thickness in non-growth region			
$t_{S=0.9}$	nm	Thickness in the desired growth region when			
		S = 0.9			
$S_{t=10 \text{ nm}}$	_	Deposition selectivity when film thickness in the			
		desired growth region = 10 nm			

growth initiation on surfaces where growth is generally not desired. Model output also allows direct comparison of ASD results from different laboratories or from different material systems. The Avrami model, 19 also known as the Johnson-Mehl-Avrami-Kolmogorov model, is a well-known approach to describe isothermal nucleation and phase change as a function of time. While often used for three-dimensional transformations, it is readily adaptable to the quasi-two-dimensional problem of understanding island growth during film deposition.<sup>20</sup> While some deviations from Avrami-type nucleation are known, it is recognized to fit well to many physical systems including diffusion controlled precipitation, structural domain switching, amorphous solid recrystallization, and sputtered thin film agglomeration. <sup>21–23</sup> An approach based on the Avrami method has also been used by Lee et al.<sup>24</sup> to analyze nuclei size evolution during Pt ALD, including a useful scheme adapted here for nuclei volume integration. The work of Lee et al. 24 showed reasonable prediction of the nuclei size evolution, giving insight into Pt nucleation on two representative surfaces.

The Avrami analysis assumes randomly distributed nuclei with fixed position and effectively zero critical radius. <sup>19,20</sup> It is important to note that the Avrami approach does not specify or limit the mechanisms for film growth. As described below, this article proscribes growth to be uniform in all directions with a constant growth per cycle, as expected for ALD. In principle, other growth modes including, for example, planar growth of 2D materials or facet-preferential adsorption, or other mechanisms leading to nonspherical nuclei could also be coupled into the nucleation model by modifying the mathematical description of the growth rate.

#### A. Nucleation sites for ALD initiation

During inhibited growth, no measureable growth is observed for the first cycles, after which some small amount of growth can be detected, eventually leading to uniform coverage. As nuclei coalescence, the net measured film growth rate increases, eventually becoming equal to the rate observed on more receptive substrates. Nucleation sites on the starting surface,  $\hat{N}$  (nm<sup>-2</sup>), could correspond to contaminant atoms or other imperfections that promote reactant adsorption. The value for N could then depend, for example, on the cleaning process used for substrate preparation. Another possibility is that a defect-free surface could have  $\hat{N}$  sites present, where the sites correspond to ALD precursors physisorbed on the clean surface during the first dose cycle that remain present after the subsequent purge step. In this scenario, the value for  $\hat{N}$  could depend not only on the precursor/surface interaction chemistry at the deposition temperature, but also on the extent of precursor exposure, reactor purge conditions, and other process variables. If conditions promote a small number of precursors to stick on an otherwise clean surface, this could be a mechanism that leads to the number of nucleation sites increasing as growth proceeds, i.e.,  $\dot{N} > 0$ .

The model considers that film growth begins at a number of nucleation point sites that are fixed in position on the surface. Here, we proscribe the rate of material growth,  $\dot{G}$  (nm/cycle) to be constant, proceeding equivalently in all directions, as expected for ALD of a uniform amorphous film. When deposition proceeds at a uniform growth per cycle on an isolated nucleus, the nucleus diameter increases as  $2\dot{G} \cdot n$ , where n is the number of ALD cycles. The analysis would be the same for a CVD process, where  $\dot{G}$  is in (nm/time) and n is deposition time. Hemispherical grains join together as growth proceeds, and growth proceeds in the normal direction at rate  $\dot{G}$  on the nuclei surface. At the regions where nuclei touch, lateral growth ceases, eventually leading to full film coalescence.

The Avrami model assumes that nucleation takes place at a defined number of randomly distributed sites on the surface. For our analysis, we consider two scenarios to define these nucleation sites: (i) a fixed number of sites,  $\hat{N}$  (nm<sup>-2</sup>), are present during the first ALD cycle (i.e., they are present on the starting surface or generated quickly during ALD) or (ii) the starting surface contains no growth sites, but sites are generated as a function of cycle number (or time), with a rate of  $\hat{N}(n)$  (nm<sup>-2</sup> cycle<sup>-1</sup>)

$$\dot{N}(n) = \dot{N}_0 \exp(-\nu_d/n). \tag{2}$$

Equation (2) represents one possible functional form for  $\dot{N}(n)$ . The term  $\dot{N}_0$  is the nucleation generation rate  $(\text{nm}^{-2}\,\text{cycle}^{-1})$ , and the parameter  $v_d$  in the exponent is the characteristic number of cycles for nucleation incubation. When  $\dot{N}(n) > 0$ , the value for  $v_d$  becomes a fit parameter corresponding to the number of ALD cycles at which  $\dot{N}(n) = \dot{N}_0/e$ . When sites are generated, the Avrami method restricts site generation to only be on exposed areas where no growth is present, so that the net rate of site generation will decrease as growth proceeds. Future work may identify other functional forms for Eq. (2) that are more appropriate for specific materials or processes.

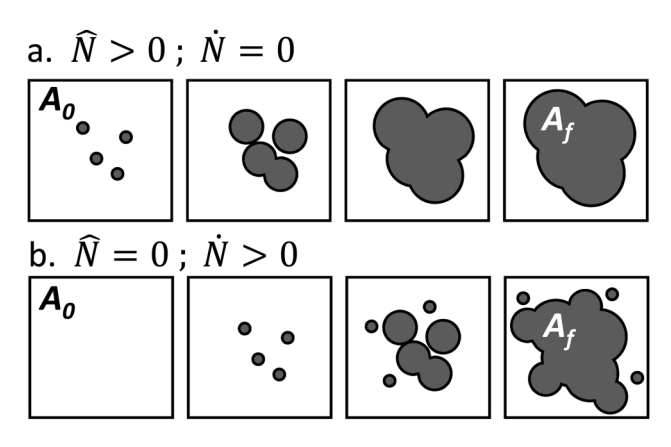


Fig. 2. Top-view schematic of nuclei on a substrate surface as growth time proceeds from left to right. *Top row:* Nucleation sites present on the starting surface grow in size as deposition proceeds. *Bottom row:* A pristine starting surface shows continuous nucleation site generation and growth as deposition proceeds.

A schematic top view of the nuclei coverage under two limiting cases: (i)  $\hat{N} > 0$  and  $\dot{N} = 0$  and (ii)  $\hat{N} = 0$  and  $\dot{N} > 0$ , is shown in Fig. 2. For any cycle number n, the fraction of the planar substrate surface area  $A_0$  that is covered by film is  $A_f/A_0$ , where  $A_f$  corresponds to the area of the film in contact with the substrate. Note that  $A_f$  is less than the total exposed (i.e., top) surface area of the deposited film. On all film regions on the substrate, the film growth continues at rate  $\dot{G}$  in the direction perpendicular to the growth surface.

#### B. Avrami model for surface coverage

The model presented here will give us an analytical relation for the geometric fraction of the starting substrate surface covered by growing film  $A_f/A_0 = \theta$ , as a function of ALD growth cycles or time, for any values of the parameters  $\hat{N}, \dot{N}_0$ ,  $v_d$ , and  $\dot{G}$ . The value for  $A_f/A_0$  could be directly measured, for example, by plan-view SEM. To characterize and quantify the extent of selectivity, the values of  $A_f/A_0$  will be used to determine the expected net "thickness" of deposited film on the desired non-growth surface as a function of the number of ALD cycles, referred to as  $t_{ng}$ . In this analysis, the calculated thicknesses correspond to the volume of deposited material per unit surface area of the underlying substrate.

To calculate  $A_f/A_0$ , we first find the extended area,  $A_e$ , defined as total area of a flat surface covered by the nuclei after n deposition cycles if the nuclei were allowed to grow without overlapping. After a small number of cycles,  $A_e = A_f$ , but after many cycles  $A_e$  will necessarily take on the non-physical condition that  $A_e > A_f$ . To find  $A_e$ , we fix a value for n, the number of ALD growth cycles (or CVD growth time) from n = 0 to  $n_{\text{max}}$  ( $n_{\text{max}}$  is the total number of cycles studied) and then find the extended area for all nuclei present after that number of cycles. Consider first the extended area due to growth on  $\hat{N}$  (nm<sup>-2</sup>) nucleation sites present on the growth surface. After n cycles, if nuclei do not overlap, each growth site will have grown into a circle with radius =  $\hat{G} \cdot n$ . The extended area resulting from  $\hat{N}$  sites is the product of

the area of each nucleus,  $\pi(\dot{G}n)^2$  and the number of nuclei present,  $A_0\hat{N}$ 

$$A_{\rho\hat{N}} = \pi (\dot{G}n)^2 \cdot A_0 \hat{N}. \tag{3}$$

We also must calculate the extended area due to nuclei generated during deposition,  $A_{e\dot{N}}$ . If a nucleus starts to grow at cycle = v, then after cycle number n > v, it covers an area  $\pi[\dot{G}(n-v)]^2$ . Note that cycle numbers before the nucleus were generated (i.e., where n < v are excluded to ensure that the extended area is positive). At cycle n, the number of nuclei present on the surface is the number present initially,  $\hat{N}$ , plus the total number generated from cycle = 0 to n:  $\int \dot{N}(n)\partial n$ . To find the extended area due to generated nuclei, we need to find the number of nuclei that started growing at an arbitrary cycle number v < n. The number that started growing at cycle = v is the number generated between v and  $v + \partial v$ . From Eq. (2)

$$\dot{N}(n)\partial v = \dot{N}_0 \exp(-v_d/v) \, \partial v, \tag{4}$$

where  $v_d$  is the characteristic number of cycles for nucleation incubation.

To find  $A_{e\dot{N}}$ , we fix a value of n from 0 to  $n_{\text{max}}$ , then, for each value of v between 0 and n, we find the extended area for all nuclei generated at that v

$$\partial A_{e\dot{N}}(n) = \pi \left[ \dot{G}(n-v) \right]^2 \cdot A_0 \dot{N}_0 \exp(-v_d/v) \cdot \partial v.$$
 (5)

Integrating the extended areas over v between 0 and n, we then obtain the total extended area at cycle n due to nuclei generated during growth. Adding to this number the extended area due to nucleation sites present on the starting growth surface, Eq. (3), gives the desired expression for the total extended area  $A_e(n) = A_{e\hat{N}}(n) + A_{e\hat{N}}(n)$ 

$$A_e(n) = A_0 \pi (\dot{G}n)^2 \cdot \hat{N}$$

$$+ A_0 \pi \int_0^n \left[ \dot{G}(n-v) \right]^2 \cdot \dot{N}_0 \exp(-v_d/v) \cdot \partial v. \quad (6)$$

The Avrami relation is then used to assert that during a period  $v + \partial v$ , the change in film coverage area,  $\partial A_f$ , is directly proportional to the change in the extended area,  $\partial A_e$ , where the proportionality factor is the fraction of surface that is not covered by film

$$\partial A_f = \partial A_e (1 - A_f / A_0). \tag{7}$$

Separating variables and integrating Eq. (7) gives

$$A_f/A_0 = 1 - \exp(-A_e/A_0).$$
 (8)

We can now substitute  $A_e(n)$  from Eq. (6) into Eq. (8) and find  $A_f(n)/A_0$ , the fraction of the growth surface covered by film versus ALD cycles (or growth time). Figure 3 shows plots for  $A_f/A_0$  as a function of ALD cycles calculated from Eq. (8) for various values of  $\hat{N}$ ,  $\dot{N}(n)$ , and  $\dot{G}$ . The expected thickness versus cycle on the desired growth and non-growth surface for each condition is also plotted in Fig. 3, as discussed below.

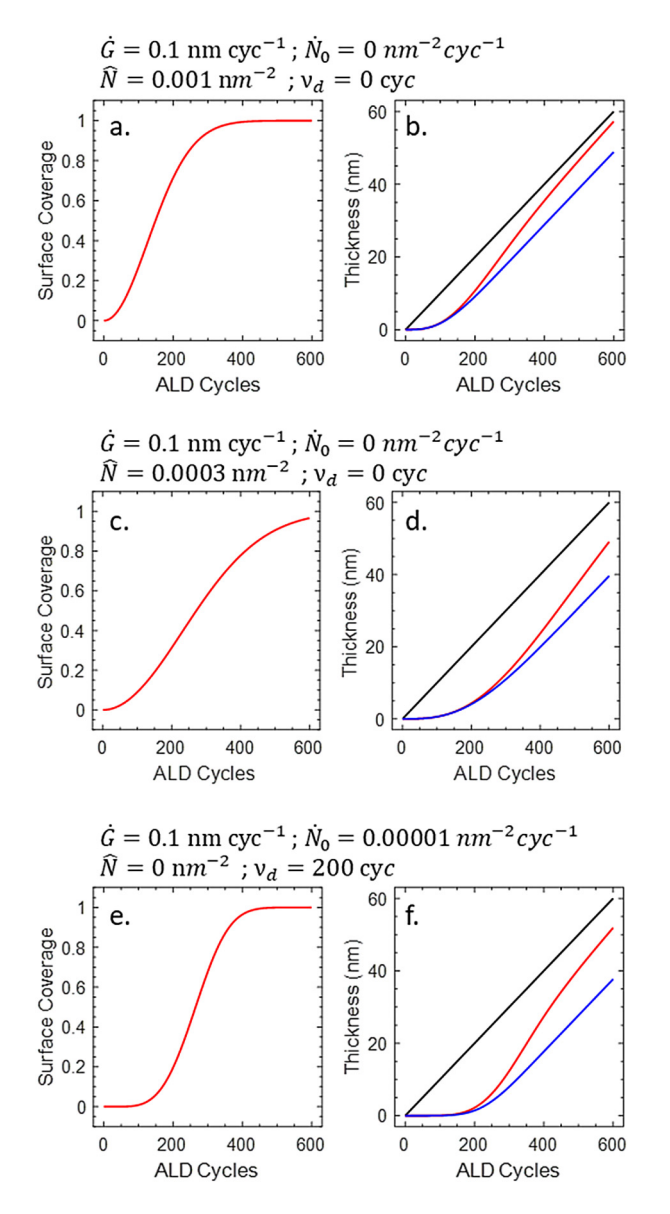


Fig. 3. Model output showing surface coverage as a function of ALD cycles and expected film thickness on the desired growth surface (black lines) and on the non-growth surface (red and blue lines) for several values of model input parameters. The red lines correspond to the output from the full integral model, and the blue lines are from the simplified model described in the text.

During experimental analysis of area-selective deposition, data sometimes include surface coverage fraction as a function of growth cycles, collected using microscopy (i.e., SEM) or spectroscopy (i.e., Auger or XPS). The values for  $A_f/A_0$  that come from the model (in Fig. 3) would correspond to data collected, for example, by plan-view SEM. To compare the model to spectroscopic atomic fraction data, one must adjust the data (or the model) using the expected escape depth of the species detected (i.e., photoelectrons or Auger electrons). When the thickness of the deposited nuclei is less than or close to the escape depth, the measured deposited fraction will underestimate the fractional surface coverage. This is discussed in more detail below with Fig. 7 and Eq. (17).

### C. Film volume deposited per area per cycle (simple approximation)

The motive of this work is to create a model that is simple to use to characterize experimental ASD results. Most ASD experiments measure the film deposited on the desired growth and inhibited (non-growth) surfaces as a function of cycles. For dielectric films, ellipsometry provides a measure of the average amount of film deposited over the measurement area. Ellipsometry can also be used to probe initial nucleation of metals, but analysis usually requires normalization or correlation to another independent thickness measurement. To correlate the nucleation model to growth rate data, the values of  $A_f/A_0$  versus cycles obtained from Eq. (8) are used to determine the net amount of material deposited versus cycle number. The data are then compared to the model output and the model parameters are adjusted to obtain a reasonable fit.

Section III D below describes a full analysis to determine the net material deposited on the desired growth surface versus cycle number for any choice of input parameters. The numerical solution requires performing a double-nested numerical integration of the fractional surface coverage. To provide a simpler option for the mathematical analysis, we note that during early stages of film deposition, the amount of film growth is proportional to the fractional surface coverage. For an isolated hemispherical nucleus with radius r (i.e., when  $A_f/A_0$  is small), the exposed top area of the hemisphere where the deposition occurs is  $2\pi r^2$ , which is  $2\times$  the area of the circle that the hemisphere covers. For this condition, the volume of film deposited per unit covered area per cycle is  $2 \cdot (A_f/A_0)G$ . After full film coalescence  $(A_f/A_0 = 1)$ , the surface area flattens out, so the growth area equals the substrate area and the volume deposited per unit area per cycle approaches  $(A_f/A_0)G$ . From this, the total growth area per unit of covered substrate area can be roughly approximated as  $[2 - (A_f/A_0)]$ . Therefore, after any cycle, n, the approximate volume of material deposited per unit substrate area on the non-growth surface (i.e., approximate average film thickness,  $\tilde{t}_{ng}$ ) is given by

$$\tilde{t}_{ng}(n) = \frac{1}{A_0} \int_0^n \left(2 - \frac{A_f}{A_0}\right) A_f \dot{G} \, dn,$$
(9)

where the value for  $A_f/A_0$  is a function of (n), as obtained from the solution to Eq. (8). While this simplified form for the film volume deposited per unit area follows the full model trend during initial film growth (as described below), the simple model deviates from the full model in the regime where the nuclei coalesce. Therefore, the simplification should be used carefully when analyzing full film thickness evolution results. This simplified model, including the calculation of  $A_f/A_0$  and a numerical integration to obtain  $\tilde{t}_{ng}(n)$ , can be implemented in a simple spread-sheet calculation for any set of values for  $\hat{N}$ ,  $\hat{N}_0$ ,  $v_d$ , and  $\dot{G}$ . The value of  $\dot{G}$  is determined directly from the measured thickness per cycle on the desired growth surface. This leaves  $\hat{N}$ ,  $\dot{N}_0$ , and  $v_d$  as the adjustable parameters in the model fit. Figures 3 and 4 show model result

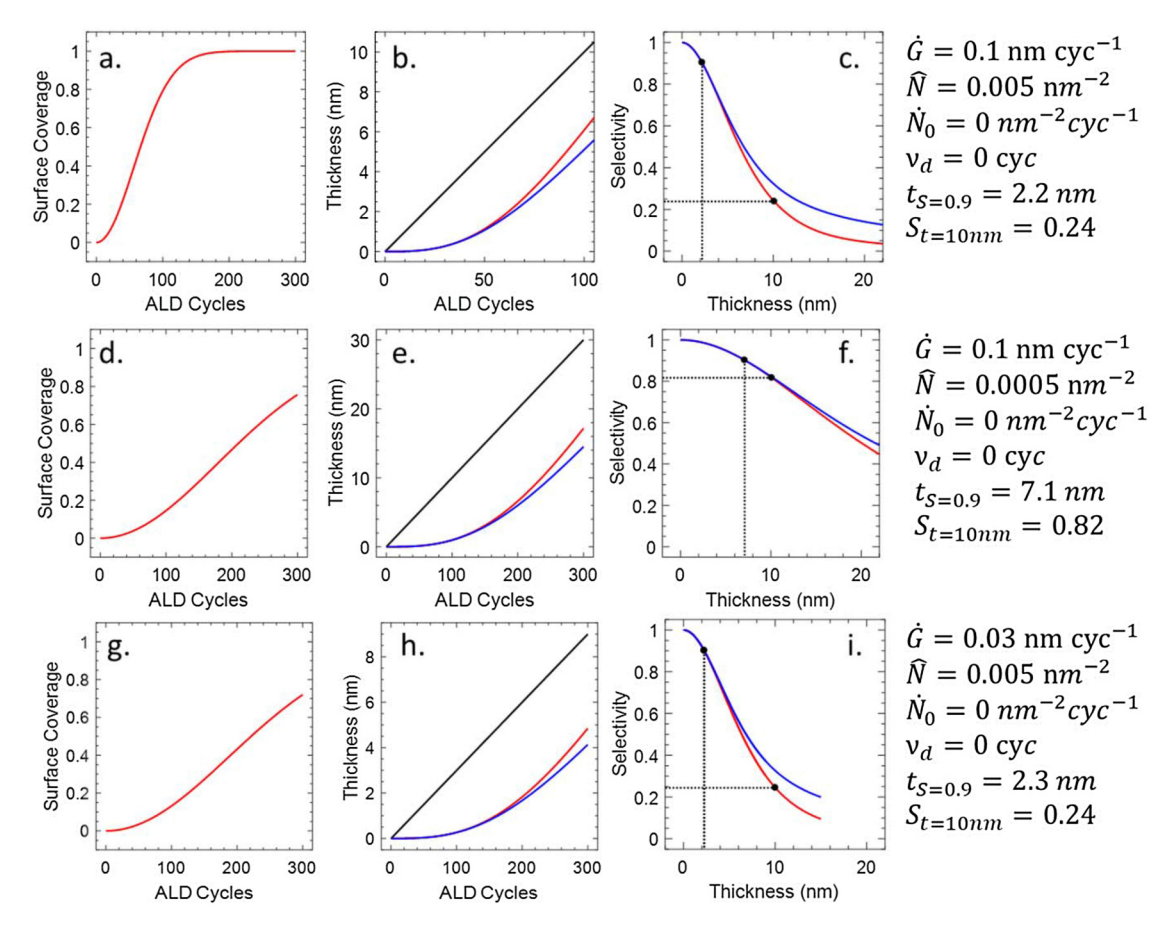


Fig. 4. Model output of surface coverage and film thickness vs ALD cycles, and selectivity as a function of film thickness on the desired substrate surface for three different sets of model input parameters. The red and blue lines correspond to the full integral model and the simplified model output, respectively. The different model parameters lead to different surface coverage and selectivity. The plots of thickness vs ALD cycles in panels (b), (e), and (h) are drawn in different scales to highlight the concept that thickness curves that appear similar can represent very different selectivity results.

for thickness versus cycle using example values for of  $\hat{N}$ ,  $\dot{G}$ ,  $\dot{N}_0$ , and  $v_d$ . In these figures, the blue lines correspond to the approximate thickness from Eq. (9), and the red lines show the full model outcome using the same model parameters, as described below. The trends in Figs. 3 and 4 are described below, after discussion of the full analytical nucleation model.

### D. Film volume deposited per area per cycle (full analysis)

To determine the amount of film deposited versus ALD cycles, we need to consider deposition that occurs on nucleation sites present on the starting surface and nucleation sites generated as growth proceeds. For nuclei present or generated at random locations across as surface, we can determine the extended nuclei area that coincides with a plane at height h above the substrate, assuming the nuclei do not touch. We then can use the Avrami relation to determine the actual area at height h for intersecting nuclei and integrate those areas over all values of h to determine the net deposition volume. We note that for an isolated hemispherical nucleus with radius (and therefore height) r, a plane intersecting the nucleus horizontally at height h above the substrate will subtend an area  $A_f(h) = \pi (r^2 - h^2)$ . The volume of the hemispherical film

nucleus is the sum of discs with area  $A_f(h)$  and thickness dh evaluated at each h from h = 0 to r

$$V_f = \int_0^r A_f(h) \,\partial h = \int_0^r \pi \,(r^2 - h^2) \partial h. \tag{10}$$

For a single isolated nucleus, we can readily confirm this equation by analytically solving the integral to obtain  $V_f = (2/3)\pi r^3$ , the expected relation for volume of a hemisphere. For randomly distributed and intersecting nuclei, the integration becomes more complex. However, the volume can be solved by calculating  $A_f(n,h)$ , analogous to that done above in relation to Eq. (8). This requires calculating the extended area as a function of height, h, above the substrate for nuclei that form at sites generated during growth,  $A_{e\hat{N}}$ , and for nuclei that start to grow immediately on the starting non-growth surface,  $A_{e\hat{N}}$ .

We first note that for an ALD process, the radius and height of an isolated nucleus is  $r = \dot{G} \cdot n$ , where  $\dot{G}$  is the growth thickness per cycle and n is the number of cycles. Then, to find the extended area after cycle n at any height h due to sites generated during deposition,  $A_{e\dot{N}}(n,h)$ , we use the relation for extended area  $A_{e\dot{N}}(n)$  in Eq. (6), and following the expression in Eq. (10), replace the  $\pi r^2$  term with  $\pi(r^2 - h^2)$  [i.e.,  $\pi \dot{G}^2(n - v)^2$  becomes  $\pi [\dot{G}^2(n - v)^2 - h^2]$ ]

$$A_{e\dot{N}}(n,h) = \begin{cases} A_0 \pi \int_0^n (\dot{G}^2(n-v)^2 - h^2) \dot{N}_0 \exp(-v_d/v) \, \partial v \\ 0 \end{cases}; \quad h \le \dot{G}(n-v), \\ ; \quad h > \dot{G}(n-v).$$
 (11)

In this expression, the parameters n and v are the ALD cycle number and the cycle number at which the nucleus being analyzed was formed, respectively. To numerically solve Eq. (11), we fix a value of n from 0 to  $n_{\text{max}}$  (the total number of ALD cycles used) and then select a height h. For that cycle and height, we calculate the extended area for each nucleus that started to grow at cycle v. The values for h and v are restricted so that  $h \leq \dot{G}(n-v)$ . That is, the horizontal plane at height h must be low enough to ensure that it intersects with the nucleus whose tallest point reaches G(n-v). For any values of v, h, and n that meet this condition, the total extended area is the product of the number of nuclei present,  $A_0\dot{N}_0\exp(-v_d/v)$  , and the area of each nucleus at height h,  $\pi[\dot{G}^2(n-\nu)^2-h^2]$ . At the specified  $\dot{G}$ , using fixed values for h and n, this product is integrated over the appropriate range of v as shown in Eq. (11) to give  $A_{e\dot{N}}(n,h)$ , the extended area at height h after cycle n resulting from nuclei generated during growth. In the integral, values of  $\nu$  that correspond to  $h > \dot{G}(n-v)$  will contribute negative values to the extended area, so as shown in the 2nd line of Eq. (11), those values are explicitly eliminated from the integration.

To find  $A_{e\hat{N}}(n,h)$ , the extended area at cycle n at any height h due to nucleation sites present on the starting surface, we make the same substitution into Eq. (6) as discussed above for Eq. (11). That is, the term  $\pi(\dot{G}n)^2$  in Eq. (6) is replaced with  $\pi(\dot{G}^2n^2-h^2)$  to give  $A_{e\hat{N}}(n,h)=A_0\pi~(\dot{G}^2n^2-h^2)\hat{N}$ . Then, adding  $A_{e\hat{N}}(n,h)$  to the value of  $A_{e\hat{N}}(n,h)$  obtained from Eq. (11), we find the total extended area at height h above the substrate after n deposition cycles

$$A_e(n,h) = A_0 \pi \ (\dot{G}^2 n^2 - h^2) \hat{N} + A_{e\dot{N}}(n,h). \tag{12}$$

Using the value  $A_e(n, h)$  from Eq. (12), we follow the Avrami relation in Eqs. (7) and (8) to calculate value for  $A_f(n, h)$ , the area subtended by a plane at height h intersecting random isolated and coalesced nuclei present after cycle n on a substrate with area  $A_0$ 

$$A_f(n,h) = A_0[1 - \exp(-A_e(n,h)/A_0)]. \tag{13}$$

To find the net volume of deposited film at cycle number (or time) n, the integration in Eq. (11) and the conversion in Eq. (13) need to be repeated for every value of h from 0 to  $h_{\text{max}} = \dot{G} \cdot n$ . This produces a set of values for  $A_f(n, h)$ , and integrating these values gives the net volume of film deposited after cycle n

$$V_f(n) = \int_0^{h_{\text{max}}} A_f(n, h) \, \partial h. \tag{14}$$

The value of  $dh = \dot{G} dn$  is the thickness of film deposited per cycle on the desired growth surface. The average film thickness on the desired non-growth surface at cycle n:  $t_{ng}(n)$  is

found by uniformly distributing the calculated film volume over the unit surface area  $A_0$ 

$$t_{ng}(n) = \frac{1}{A_0} V_f(n). \tag{15}$$

These equations can be developed and solved in mathematical software, such as MATLAB® to analyze results from studies of ALD nucleation and/or area-selective deposition (see supplementary material). By selecting values for input parameter  $\dot{G}$ ,  $\dot{N}$ ,  $\dot{N}_0$ , and  $v_d$ , output from the model can include: expected fractional surface coverage on the nucleating non-growth surface versus ALD cycle; expected measured thickness on the growth and non-growth surface versus cycle; number of nuclei present versus cycle number, and other parameters of interest. Example model results are described below.

#### E. Trends in model output

Figures 3 and 4 show an example model output for several example input parameter sets. In each plot, the red lines correspond to the full model analysis from Eqs. (11)–(14) and the blue lines correspond to the simplified solution from Eq. (9). The plots in Fig. 3 show output for a fixed value of G, with  $\hat{N} > 0$  and  $\hat{N} = 0$ , as well as for  $\hat{N} = 0$  and  $\hat{N} > 0$ . Comparing plots in Figs. 3(a) and 3(c) shows that decreasing the value of  $\hat{N}$  from  $1 \times 10^{-3}$  to  $3 \times 10^{-4}$  nm<sup>-2</sup> leads to a larger number of cycles needed to achieve full surface coverage on the non-growth surface. Similarly, in Figs. 3(b) and 3(d), decreasing  $\hat{N}$  leads to a longer delay before film appears in the non-growth region. When nucleation sites are generated during growth,  $\hat{N} > 0$ , with  $\hat{N} = 0$  [Figs. 3(e) and 3(f)], the transition to full coverage occurs more quickly, and the appearance of film in the non-growth region happens more abruptly compared to when N = 0 and N > 0. This model output therefore follows the expected intuitive trend that fewer nucleation sites, either present on the starting surface or generated during growth, will prolong the appearance of unwanted film growth, which will improve overall selectivity.

Figure 4 presents another set of model output curves generated using a different set of input parameters for  $\dot{G}$ ,  $\hat{N}$ ,  $\dot{N}_0$ , and  $v_d$ . For this set, a quick look at the panels in the middle column [Figs. 4(b), 4(e), and 4(h)] may suggest nearly the same trend in unwanted film growth versus cycle for each parameter set. However, closer examination shows that these plots have different scales on the x- and y-axes. The model output shows that each set gives different trends for expected surface coverage [Figs. 4(a), 4(d), and 4(g)]. Also, the calculated trends in selectivity (defined in Sec. IV) show different trends for each condition, as shown in Figs. 4(c), 4(f), and 4(i). The parameter set giving the best selectivity is given in the middle row of Figs. 4(d), 4(e), and 4(f). The improved selectivity in Fig. 4(e) relative

to Figs. 4(d) and 4(h) becomes apparent if all plots were presented with common axis scales.

In the thickness versus cycle plots in Figs. 3 and 4, the approximate and full model output (blue and red lines for  $\tilde{t}_{ng}$  and  $t_{ng}$ , respectively) have a slope (growth per cycle) that increases, eventually reaching the slope of the black line,  $\dot{G}$ , the growth rate observed on the desired growth surface. Figure 3(b) shows most clearly that the blue, red, and black lines approach a common slope after a large number of cycles. More importantly, all plots show that the approximate and full models overlap in the region where the amount of film deposited is relatively small, before the nuclei begin to coalesce. Fortunately, as discussed below, the region where the amount of film deposited is small is also the region of interest to quantify the selectivity. Therefore, the simple model can be a useful approximation to the fully integrated solution to compare selectivity of different data sets.

### F. Deposition thickness per ALD cycle and slope of the thickness versus cycle plots

Even though the deposited thickness per ALD cycle is constant throughout the deposition process, the model appears to show a regime on the nucleating non-growth surface, where the slope of thickness  $t_{ng}$  versus cycle exceeds that for the steady-state ALD rate on the growth surface, G [e.g., the red lines in Figs. 3(b), 3(d), and 3(f) between 200 and 400 cycles]. To understand this, consider the amount of film deposited during a single ALD cycle on an isolated hemispherical nucleus. On a hemisphere with radius r, the exposed top surface where growth occurs has a surface area of  $2\pi \cdot r^2$ , which is  $2\times$  larger than the circular area that the nucleus covers on the substrate. This means that for a fixed deposition thickness per cycle, the volume of material deposited per cycle on the nucleus is 2× larger than on a flat surface covering the same substrate surface area. Most experimental measurements of film thickness probe material volume per unit substrate surface area; quartz crystal microbalance measures film mass, Rutherford backscattering measures number of deposited atoms, and ellipsometry analyzes the film and film/substrate optical response and fits it to a model that outputs a thickness value. Therefore, on a nonplanar surface, a given ALD thickness per cycle will produce a measured thickness per cycle (i.e., volume per unit substrate area per cycle) that appears to be larger than that for the same process on a planar surface. This enhancement is most operative when the nuclei are isolated, but it is not readily visible during early growth with few nuclei, because the total amount of material deposited per cycle is very small. The effect becomes most pronounced during nuclei coalescence when the surface is nearly fully covered by many nuclei. After coalescence, the film smoothens out during growth, so the measured growth per cycle returns to its expected steady-state value.

The red lines in Figs. 3(b), 3(d), and 3(f) correspond to the expected thickness versus cycle when fixed hemispherical nuclei grow and coalesce into a continuous film. If the nuclei are nonhemispherical, i.e., due to crystallization or differences in nucleus/substrate interfacial energy, or if atom clusters

diffuse on the surface,  $^{12}$  the form used for growth rate,  $\dot{G}$ , would need to be modified in the model to accommodate these effects. If any mechanism is present to "flatten" the hemispherical nuclei, then the resulting data would be expected to follow a trend between the red and blue lines.

When nuclei are generated during growth, the surface has a relatively large number of small nuclei, leading to a more pronounced enhancement in the apparent growth rate. This is shown in thickness plots in Figs. 3(b), 3(d), and 3(f), where the slope change in Fig. 3(f) with  $\dot{N} > 0$  is larger than for  $\dot{N} = 0$  in Fig. 3(b). Comparing the output from the simplified and full model (blue and red lines, respectively) shows that the simplified model does not capture the apparent enhanced thickness per cycle. Otherwise, the output from Eq. (9) coincides well with the full model output from Eq. (14).

#### G. Analysis of nucleation using ellipsometry

Ellipsometry is convenient to analyze dielectric film thickness, and it is used for some of the examples shown below. When using ellipsometry, collected data are generally compared and fit to an optical model including parameters for the materials on the surface, thereby providing estimates for film thickness and optical constants. If the optical model presumes a continuous thin film, then a discontinuous nucleating film will generally not provide accurate estimates for optical constants and thickness. It is important therefore to not "over-interpret" ellipsometry thickness results, especially for data collected during film nucleation and early film growth. Improved analysis of nucleation using ellipsometry may come from direct reporting and characterization of raw ellipsometry data (i.e., change in  $\Psi$  and/or  $\Delta$  parameters versus deposition cycle) as films grow. Future work could modify the model presented here to create output for expected values for ellipsometry parameters, allowing direct comparison with measured raw ellipsometry data.

### IV. QUANTITATIVE ANALYSIS OF NUCLEATION AND AREA-SELECTIVITY IN ASD

### A. Selectivity versus film thickness in desired growth region

As discussed above, Eq. (2) gives a numerical definition for overall selectivity during film deposition. For the analysis below, we work under conditions where the fractional surface coverage in the desired growth area,  $\theta_1$ , quickly reaches a value of one. However, the model can also be readily adapted to cases where some delay also occurs on the desired growth surface. As growth proceeds and unwanted film begins to cover desired non-growth surface, the surface coverage on the desired non-growth surface is  $\theta_2 = A_f/A_0$ . Setting  $\theta_1 = 1$  and substituting  $\theta_2 = A_f/A_0$ , Eq. (1) becomes

$$S(n) = \frac{1 - \theta_2}{1 + \theta_2} = \frac{1 - A_f / A_0}{1 + A_f / A_0},$$
 (16)

where it is explicitly noted that the value of S depends on n, the number of ALD cycles (or CVD deposition time). When

the film grows on the desired growth surface with no deposition in the non-growth region, then  $(A_f/A_0)=0$  and S=1, i.e., selectivity is perfect. As the desired film grows, and the film begins to appear in the non-growth region,  $A_f/A_0$  will increase, and therefore S will decrease. When the non-growth region becomes completely covered,  $(A_f/A_0)=1$  and S=0.

Using input parameter values, the analytical model gives corresponding values for  $A_f/A_0$  versus ALD cycles (or deposition time) on the non-growth surface, and S(n) is directly found using Eq. (16). Using the known deposition rate per cycle, G, we can readily plot S versus film thickness in the desired growth region,  $t_g$ . Several example plots of  $S(t_g)$  are given as the red lines in Figs. 4-8. Since the calculated thickness is different for the approximate and full integration, the model also produces plots of  $S(\tilde{t}_g)$ , shown as the blue lines in the selectivity plots. In Fig. 4(c), the input parameters give a value for  $S(t_g)$  that decreases from 1 to 0.24 when the film thickness in the desired growth region reaches 10 nm. Similarly, the output red line shows that deposition of 2.2 nm in the desired growth region would correspond to S = 0.9. In Fig. 4(f), the model parameters lead to S = 0.82 after 10 nm of growth and 7.1 nm at S = 0.9. In Fig. 4 therefore, the conditions in the middle row show overall improved selectivity relative to those in the first row. The values of  $S(\tilde{t}_g)$  from the approximate model lead to the same general conclusion, i.e., parameters in the middle row are more favorable for ASD than the top row. This is reasonable since the plots in Figs. 4(a), 4(b), and 4(c) were generated using a value for  $\hat{N}$  that is  $10 \times$  larger than in Figs. 4(d), 4(e), and 4(f). However, the significant difference in selectivity is not readily obvious by comparing the trends in thickness versus cycle in Figs. 4(b) and 4(e), which is often the type of data presented in experimental ASD studies.

### B. Definition of selectivity demarcation values $t_{s=XX}$ and $S_{t=YYnm}$

The selectivity curves obtained from the data analysis allows different ASD processes, approaches, and materials to be quantitatively compared and evaluated. To compare data from different experiments, it is useful to define a figure-of-merit or demarcation parameter that classifies the observed results. Two possible demarcation parameters are defined here. One is  $t_{S=XX}$ , the film thickness in the desired growth region that the process would enable for a selectivity value of S=XX. The second demarcation point,  $S_{t=YYnm}$ , is the selectivity value that would be obtained if one deposited YY nm of film in the desired growth region.

A general goal in ASD is to deposit a desired amount of material while maintaining a minimum threshold for unwanted growth. A threshold can be defined in many ways, but it often includes a maximum number of particles (i.e., unwanted nuclei) that are smaller than a given size. For example, a target for a selective process may be to achieve 20 nm of film in the desired growth region while

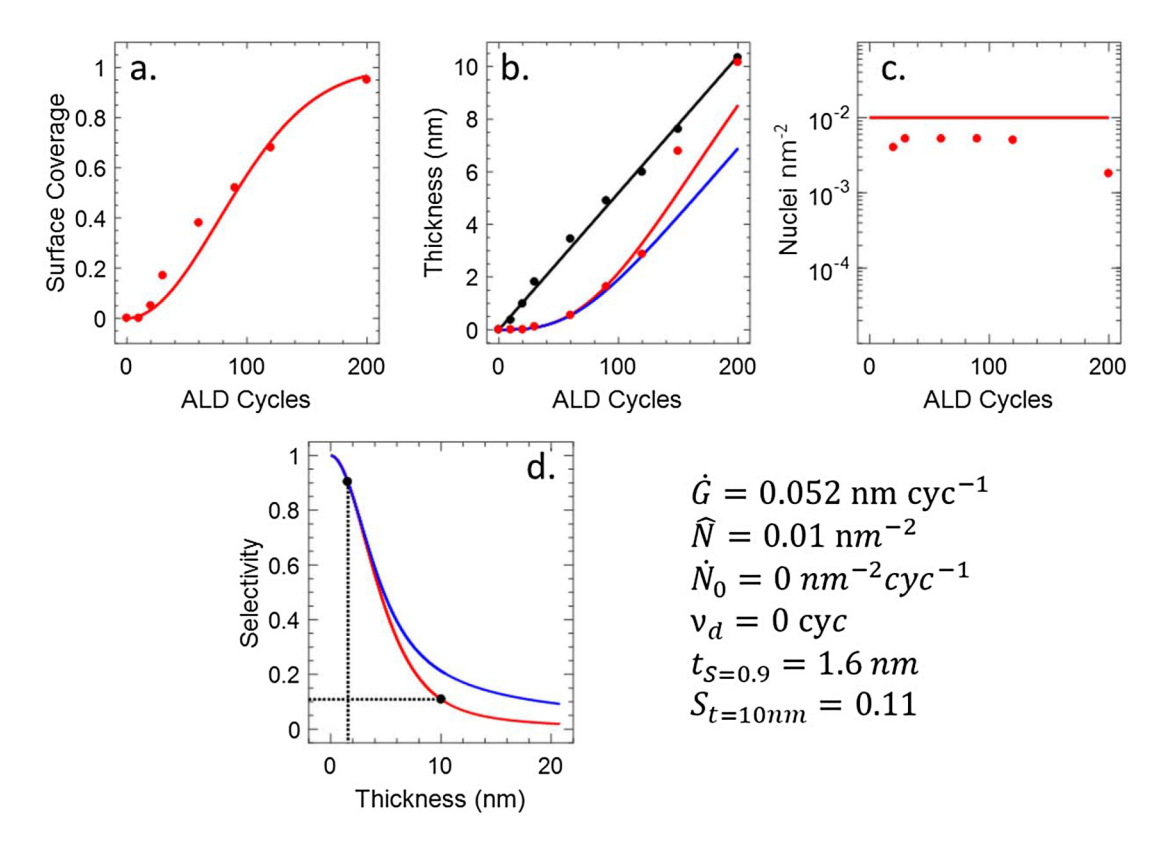


Fig. 5. HfO<sub>2</sub> ASD experimental results from Ref. 25, along with model output fits. The growth rate on the desired growth surface [black points and line in panel (b)] provides the growth rate parameter,  $\dot{G}$ , input to the model. Then, by adjusting  $\hat{N}$  as a single model parameter variable, the trends in model output correspond well to three unique sets of data collected from three different measurements on the deposited samples. The model indicates that this process could produce 1.6 nm of deposition on the desired growth surface with a selectivity of 0.90.

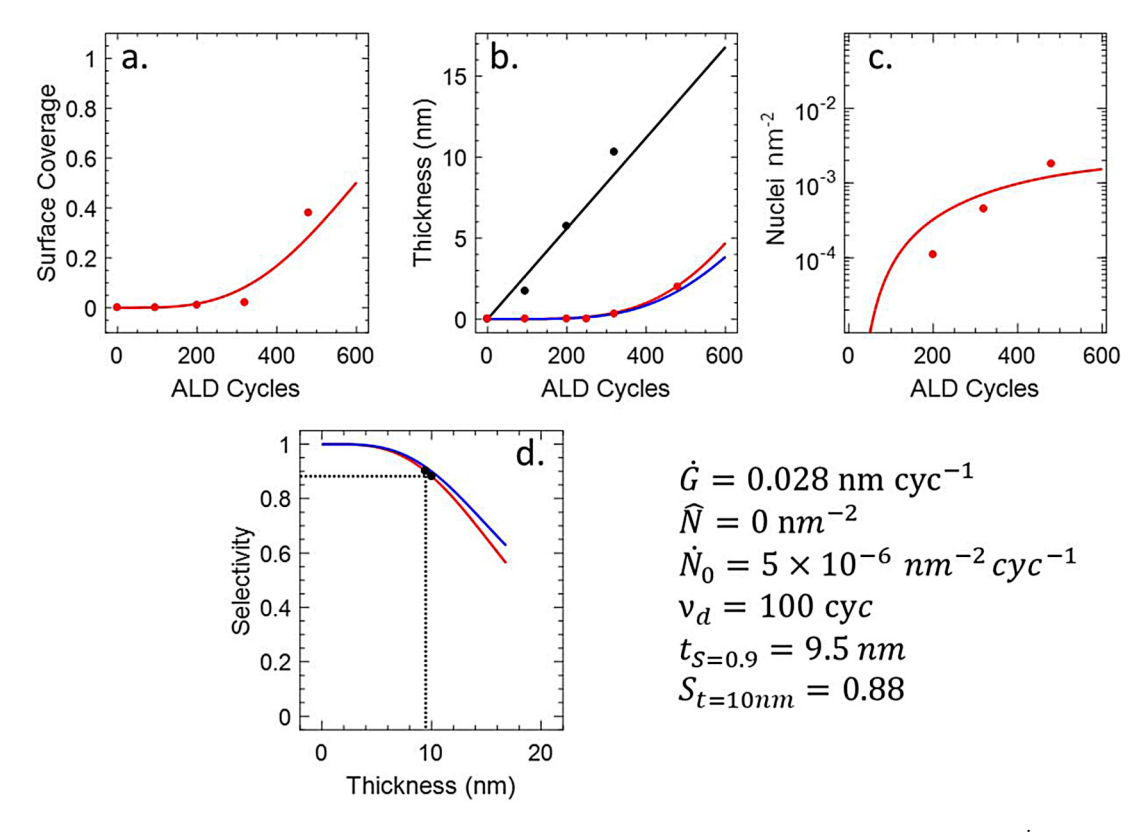


Fig. 6. TiN ASD experimental results from Ref. 25, along with model output fits. Using the growth rate data in panel (b) to find  $\dot{G}$ , the values of  $\dot{N}_0$  and  $v_d$  were adjusted to attain the fit lines shown. In this case, model output with  $\dot{N}=0$  did not show satisfactory fits. As in Fig. 4, the trends in model output correspond well to three unique sets of data collected from three different measurements on the deposited samples. The model indicates that this process could produce 10 nm of deposition on the desired growth surface with selectivity of 0.88.

maintaining <10<sup>6</sup> nuclei particles per cm<sup>2</sup> (i.e.,  $10^{-8}$  nm<sup>-2</sup>) with diameter less than 100 nm in the non-growth region. Using these parameters, the maximum allowable fractional surface coverage is found to be  $\theta_2 = (10^{-8} \text{ nm}^{-2} \times \pi \times 50^2 \text{ nm}^2) \approx 8 \times 10^{-5}$ . Using Eq. (16), with full coverage in the desired growth region, these threshold parameters correspond to  $S \approx 0.9998$  (i.e., "nearly 4-nines selectivity"). Therefore, a useful parameter to compare ASD processes for this application could be  $t_{S=0.9998}$ , i.e., the thickness a process can achieve while staying within the particle coverage threshold. Another useful parameter may be  $S_{t=20nm}$ , the selectivity (or particle density) a process achieves when the target thickness (i.e., 20 nm) is reached in the desired growth region.

To demonstrate how these demarcation values come out of the model, and how they are useful to compare different data sets,  $t_{S=0.9}$  and  $S_{t=10 \text{ nm}}$  were selected as example demarcation values. They are used to compare hypothetical ASD data as well as data published in literature, as shown in Figs. 4–8. The value  $t_{S=0.9}$  was selected here because many published data sets for ASD show S values close to 0.9. The value  $S_{t=10 \text{ nm}}$  is used because desired film thickness of t=10 nm is currently considered a reasonable and accepted target for laboratory ASD experiments, and for applications such as that shown in Fig. 1. When fitting data to the model, the quality of the fit, and hence the uncertainty in the demarcation values, will depend on the type of data and number of data points available.

### C. Model fits to experimental data, and insight into nucleation mechanisms

### 1. Procedure for comparing model fits to experimental data

Figures 5–8 show examples of model fits to published experimental ASD data,  $^{10,11,25}$  including "two-step" and "three-step" ASD processes. Generally, we seek the simplest set of independent model parameters,  $\dot{G}$ ,  $\hat{N}$ ,  $\dot{N}_0$ , and  $v_d$ , that are consistent with the available experimental data. As a first step, the value for growth rate,  $\dot{G}$ , is determined directly from measured ALD thickness data collected on a receptive growth surface. Then, in the analysis below, the model output is compared to available data (e.g., surface coverage, thickness on non-growth surface, number of nuclei, or other results) by adjusting the value of  $\hat{N}$  keeping  $\dot{N}(n)=0$ . If the data are not reconciled with the data with  $\dot{N}(n)=0$ , then various values for  $\dot{N}_0$  and  $v_d$  are tested (usually with  $\hat{N}=0$ ) to obtain a reasonable fit, as determined by eye. Future work could include statistical analysis of the fit quality in the model sequence.

#### 2. Inherent ASD of HfO2

Figures 5 and 6 show data from Stevens *et al.*<sup>25</sup> including studies of ASD of HfO<sub>2</sub> (Fig. 5) and TiN (Fig. 6), where deposition proceeds readily on Si<sub>3</sub>N<sub>4</sub> but shows inhibited island growth on H<sub>2</sub>-plasma treated amorphous carbon. For both of the material systems, the published data include three complementary data sets: atomic coverage on the growth and

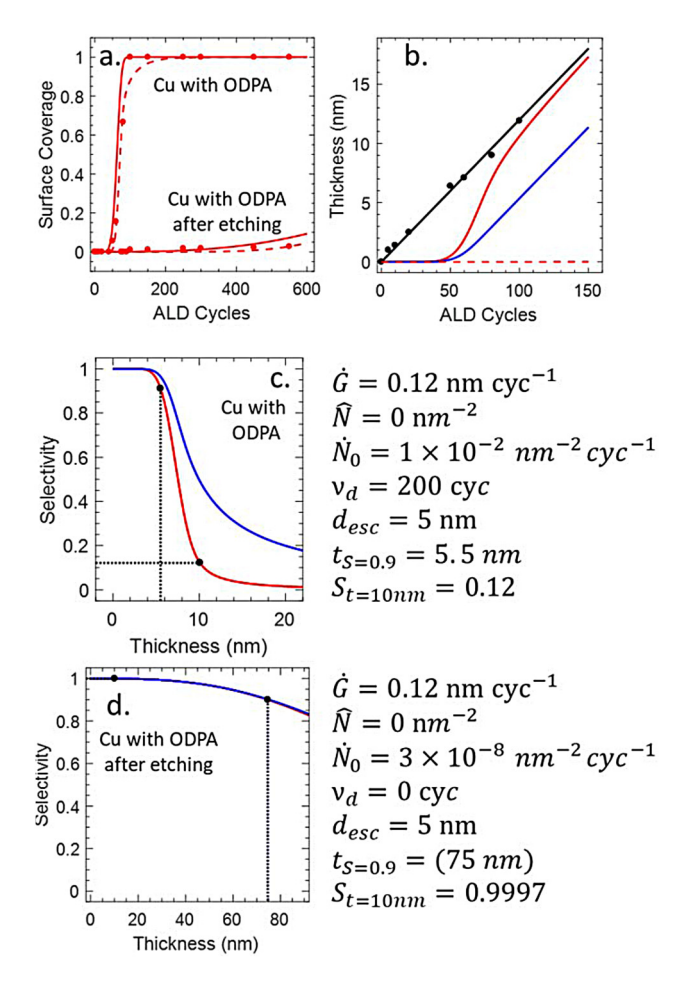


Fig. 7. Experimental results from Ref. 10, along with model output fits for ASD of  $Al_2O_3$  on  $SiO_2$ , where ODPA SAMs are used to block nucleation on Cu. Two cases are modeled, including ASD for SAMs on Cu, and ASD for SAMs on Cu treated with an additional wet etch step after ALD. The model is fit to surface coverage data collected by AES using  $\dot{N}>0$  as fits using  $\dot{N}=0$  did not correlate well with the data trends. The results show good fits to both data sets and significantly improved selectivity after the wet etch process treatment.

non-growth surfaces from RBS (which is directly converted to average thickness); fractional surface coverage from SEM; and nuclei density from SEM. Using a single set of input parameters, the model gives expected trends for all of these data sets, allowing three separate complementary checks for the model parameter values.

For the HfO<sub>2</sub> data in Fig. 5(b), the black points show measured thickness versus ALD cycles on the receptive Si<sub>3</sub>N<sub>4</sub>. The thickness values were determined from reported Hf RBS number density using the HfO<sub>2</sub> molecular weight of 210.5 g/mol and a density of 9.7 g/cm<sup>3</sup>.<sup>25</sup> The linear fit in Fig. 5(b) gives  $\dot{G} = 0.052$  nm/cycle, consistent with the value reported in the original article. The lines for the model fit were obtained by setting  $\hat{N} = 0.01$  nm<sup>-2</sup> and  $\dot{N}(n) = 0$ . While some of the data points lie off of the trend lines, overall the model output agrees well with the observed surface coverage, thickness, and number of nuclei present on the non-growth surface versus ALD cycles. Considering the data for nuclei density in Fig. 5(c), during random nucleation, some nuclei originate close together and coalesce rapidly, so the observed nuclei

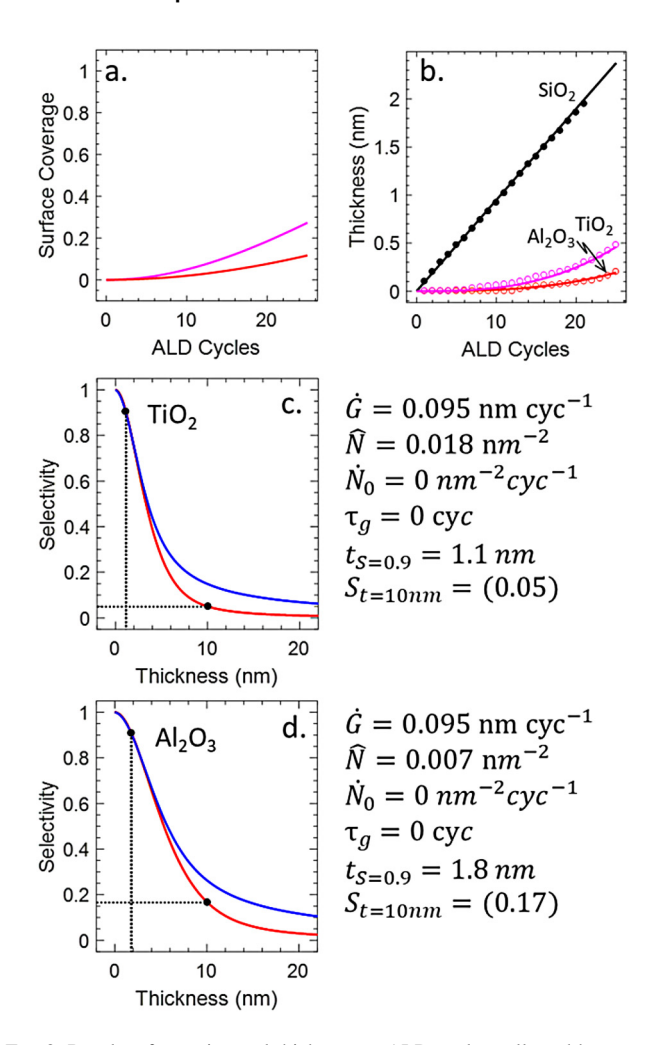


Fig. 8. Results of experimental thickness vs ALD cycles collected by in situ ellipsometry from Ref. 11, where ASD is achieved using plasma-assisted ALD with sequential exposures with a vapor-phase inhibitor. The data plots include  $Al_2O_3$  and  $TiO_2$  as non-growth substrates, and the model fits to both data sets using  $\hat{N}$  as the only adjustable model parameter.

density may be somewhat less than the true site density. The expected selectivity versus film thickness in Fig. 5(d) shows that this process could produce  $\sim$ 1.6 nm of deposition on the desired growth surface with selectivity of 0.90, and after 10 nm of deposition the selectivity would be 0.11. Note that the simplified model calculation [blue line in Fig. 5(d)] gives the same value for  $t_{S=0.9}$ , and a somewhat larger but reasonably close value for  $S_{t=10 \text{ nm}}$ .

In addition to quantitative comparison of ASD capability, the model fit in Fig. 5 also gives insight into possible ALD nucleation mechanisms in the non-growth region. For HfO<sub>2</sub>, the successful data fit to a constant nucleation density,  $\hat{N}$ , is consistent with growth beginning at nucleation sites (for example, impurities or other defects) initially present on the starting non-growth surface, with relatively few additional nucleation sites generated during film growth.

#### 3. Inherent ASD of TiN

Figure 6 shows data from Stevens *et al.*<sup>25</sup> for "two-step" ASD of TiN on  $Si_3N_4$  versus a-C, and a resulting model fit to the data. The fit to the growth rate gives  $\dot{G}=0.028$  nm/cycle,

consistent with the original report. The model output using  $\hat{N} > 0$  and  $\hat{N}(n) = 0$  showed unfavorable fits to the data. Specifically, the model showed a gradual increase in surface coverage versus time on the non-growth surface, whereas the data in Fig. 6(a) show very low surface coverage until  $\sim 250$ cycles, followed by a relatively rapid increase between 300 and 400 cycles. Also, data for nuclei density in Fig. 6(c) show values that increase with time, consistent with  $\dot{N}(n) > 0$ . Setting N(n) > 0 led to model output that more favorably agreed with the data trends. Using  $\dot{N}_0 = 5 \times 10^{-6} \text{ nm}^{-2} \text{cyc}^{-1}$ and  $v_d = 200$  cycles, the trends show good agreement for the measured surface coverage, thickness on the non-growth surface and nuclei density. The output selectivity values  $t_{S=0.9} \sim 9.5 \text{ nm}$  and  $S_{t=10 \text{ nm}} = 0.88$  indicate this TiN process has better capacity for ASD relative to the HfO2 process in Fig. 5. The values for  $t_{S=0.9}$  and  $S_{t=10 \text{ nm}}$  from the simplified model are nearly the same as from the full model analysis.

Fits for the TiN process in Fig. 6 also give insight to the nucleation mechanism. Unlike the results above for HfO<sub>2</sub>, the data fits suggest that deposition on the non-growth surface more likely begins at nucleation sites that are generated during the ALD process itself.

### 4. Surface-inhibited ASD of Al<sub>2</sub>O<sub>3</sub> with postprocess nuclei removal

Figure 7 shows data from Hashemi et al., 10 describing thermally driven ASD of Al<sub>2</sub>O<sub>3</sub> on SiO<sub>2</sub> as the desired growth surface versus Cu covered with octadecylphosphonic acid (ODPA) self-assembled monolayers (SAMs) as molecular inhibitors on the non-growth surface. The published data include Al atomic % on the non-growth surface measured by Auger electron spectroscopy as a function of deposition cycles. In Fig. 7(a), a surface coverage of 1.0 corresponds to saturated Al signal measured by AES. One data set in Fig. 7(a) was collected for a "two-step" ASD process for Al<sub>2</sub>O<sub>3</sub> ALD on patterned Cu covered with ODPA SAM inhibition layers, and it shows nearly full Al<sub>2</sub>O<sub>3</sub> coverage in the non-growth region after ~50 ALD cycles. Another data set also in Fig. 7(a) was collected for a "three-step" ASD process applying a "self-correcting" step, where the patterned sample was treated by etching in acetic acid after the Al<sub>2</sub>O<sub>3</sub> ALD step. This acid treatment removes the SAM and a majority of metal oxide deposited in the SAM region. These acid-treated samples show nearly zero Al surface coverage in the non-growth region up to 250-300 ALD cycles, with only ~1 at. % Al after 550 ALD cycles.

The surface coverage data in Fig. 7(a) were collected by AES, so for thin  $Al_2O_3$ , some Auger electrons from the underlying  $SiO_2$  could be detected. Therefore, the measured Al atom fraction will be less than the geometric fraction of the substrate that is covered by film,  $A_f/A_0$ , obtained from the model output. Comparing data from AES or x-ray photoelectron spectroscopy to modeled film surface coverage requires adjustment to the model to take into account the excited electron escape depth,  $d_{\rm esc}$ . The value will formally depend on the x-ray source energy (for XPS) and the material being analyzed (including the substrate and deposited

film), and therefore a rigorous measure of surface coverage will require estimation and integration of  $d_{\rm esc}$  across the exposed surface. If the electron escape depth  $d_{\rm esc}$  is approximately constant, and the effective film thickness on the nongrowth surface is  $t_{ng}$ , one approximation to the fractional surface coverage relative to the modeled geometric surface coverage is  $^{24}$ 

$$(A_f/A_0)_{AES} = (A_f/A_0) * [1 - \exp(-t_{ng}/d_{esc})].$$
 (17)

In Fig. 7(b), the thickness data on SiO<sub>2</sub> shows G = 0.12 nm/cycle. For the fit to the surface coverage data, any value of N with N(n) = 0 showed poor correlation to the data. Using  $\dot{N}(n) > 0$ , the solid red lines in Fig. 7(a) show the calculated values for  $A_f/A_0$  and the dashed lines correspond to  $(A_f/A_0)_{AES}$  for  $d_{esc} = 5$  nm. A smaller value for  $d_{\rm esc}$  gives a line for  $(A_f/A_0)_{AES}$  that more closely matches the solid line for  $(A_f/A_0)$ . The solid red line in Fig. 7(b) shows the expected measured thickness of Al<sub>2</sub>O<sub>3</sub> on the Cu+ ODPA substrate, and the dashed red line shows the expected trend for Cu + ODPA after etching. The selectivity plot in Fig. 7(c) corresponds to the Cu with ODPA data fit, giving  $t_{S=0.9} \sim 5.5 \text{ nm}$  and  $S_{t=10 \text{ nm}} = 0.12$ . Generally, when N(n) > 0, the slope of the selectivity plot is more abrupt than for N > 0and  $\dot{N}(n) = 0$ , and the difference between the full model calculation and the simplified model becomes more apparent, as seen by comparing Fig. 7(c) with Fig. 5(d).

Figure 7(a) also shows the fit to the data collected after the postdeposition acetic acid solution etch. The dashed line in Fig. 7(b) is the modeled  $Al_2O_3$  film thickness, and Fig. 7(d) shows the model output for selectivity versus thickness. The fit gives  $t_{S=0.9} \sim 75$  nm and  $S_{t=10 \text{ nm}} = 0.9997$ , indicating very good selectivity. While the data indicate that this process will enable 75 nm of desired film growth while maintaining  $S \ge 0.9$ , the value for  $t_{S=0.9}$  is reported in parentheses to indicate that the published experiments did not extend to films that thick.

While the model fit to data in Fig. 7 is consistent with  $\dot{N}(n) > 0$ , i.e., nucleation sites are generated at a rate that increases as ALD proceeds, one must be careful interpreting this result. For SAM-based nucleation inhibition layers, it is reasonable to expect that SAM degradation over time will allow site generation and unwanted growth, consistent with  $\dot{N}(n) > 0$ . However, the value for  $\dot{N}(n)$  obtained from the model fit corresponds to nuclei formation as well as effects of wet etching, and therefore the value for  $\dot{N}(n)$  will most likely not be related to any single quantifiable phenomenon for nucleation site generation.

#### 5. Sequential gas-phase-inhibited plasma-ASD of SiO<sub>2</sub>

Figure 8 includes data for a "three-step" plasma-assisted ASD of SiO<sub>2</sub> from Mameli *et al.*<sup>11</sup> The process uses bis(diethylamino)silane and O<sub>2</sub> plasma reactant, with additional exposure with acetylacetone as a deposition inhibitor. SiO<sub>2</sub> ALD proceeds on SiO<sub>2</sub>, GeO<sub>2</sub>, SiN<sub>x</sub>, and WO<sub>3</sub> with inhibited deposition on Al<sub>2</sub>O<sub>3</sub>, TiO<sub>2</sub>, and HfO<sub>2</sub>. The data points in Fig. 8(b) show thickness on SiO<sub>2</sub>, Al<sub>2</sub>O<sub>3</sub>, and TiO<sub>2</sub>, as determined by ellipsometry.<sup>11</sup> On SiO<sub>2</sub>, the data fit

gives  $\dot{G}=0.095$  nm/cycle. Also in Fig. 8(b), for SiO<sub>2</sub> deposition on TiO<sub>2</sub>, the model output using  $\dot{N}(n)=0$  and  $\hat{N}=0.018$  nm<sup>-2</sup> gave a good match to the data. Likewise, on Al<sub>2</sub>O<sub>3</sub>,  $\dot{N}(n)=0$  and  $\hat{N}=0.007$  nm<sup>-2</sup> gave output that matched well with the data. The resulting  $S(t_g)$  plots for SiO<sub>2</sub> on TiO<sub>2</sub> and Al<sub>2</sub>O<sub>3</sub> are given in Figs. 8(c) and (d), showing  $t_{S=0.9}=1.1$  nm and 1.8 nm for TiO<sub>2</sub> and Al<sub>2</sub>O<sub>3</sub>, respectively. Deposited SiO<sub>2</sub> thickness up to 2 nm on the desired SiO<sub>2</sub> growth surface was reported in the published data.

### 6. Discussion of data fitting analysis

The results for the example data fits in Figs. 5-8 are summarized in Table II. The example data were selected from literature to cover a generally broad set of ASD processes, including two-step and three-step methods for metals and dielectrics by thermal and plasma ALD. Processes included inherent selectivity and passivated selectivity, and the extent of selectivity in the example data ranged over several orders of magnitude, as indicated by the spread in the values for  $t_{S=0.9}$  and  $S_{t=10 \text{ nm}}$ . Furthermore, the data presented and analyzed were collected using many different characterization tools, including RBS, AES, SEM, and in situ and ex situ ellipsometry. Each example shows some differences between the data and the model. The quality of the model output will depend on the amount and experimental certainty of the data available, as well as approximations within the model. For all cases shown here, and for many other published data sets not shown, the model fits show consistent trends within individual data sets as well as between different data sets.

The data fits provide insight into possible differences in nucleation mechanisms for the different processes studied. It is interesting, for example, that the model fits for HfO<sub>2</sub> and TiN ASD data on Si<sub>3</sub>N<sub>4</sub> versus a-C performed in the same experimental system suggest nucleation sites are present on the starting surface (or generated quickly) for HfO<sub>2</sub>, whereas sites appear to be generated during TiN ALD. While the fits shown here do not definitively identify nucleation mechanisms, the model output can be used, for example, to refine experiments that test hypotheses for nucleation reactions. As noted in Sec. II, more full analysis of nucleation thermodynamics and kinetic mechanisms will require more detailed modeling. Even so, fitting experimental results to the model presented here can provide

Table II. Model input parameters and summary of fit results from the data shown in Figs. 5–8.

	Parameters							
Figure	$\dot{G}$ (nm cycle <sup>-1</sup> )	<i>Ñ</i> (nm <sup>-2</sup> )	$\begin{array}{c} \dot{N}_0 \\ (\text{nm}^{-2}  \text{s}^{-1}) \end{array}$	v <sub>d</sub> (cycles)	t <sub>S=0.9</sub> (nm)	S <sub>t=10 nm</sub> (—)		
5	0.052	0.01	0	0	1.6	0.11		
6	0.028	0.0	$5 \times 10^{-6}$	100	9.5	0.88		
7	0.12	0.0	$1 \times 10^{-2}$	200	5.5	0.12		
		0.0	$3 \times 10^{-8}$	0	(75)	0.9997		
8	0.095	0.018	0	0	1.1	(0.05)		
		0.007	0	0	1.8	(0.17)		

useful insights to improve understanding of nucleation, expand the capacity of ASD, and promote further advances in ALD and ALD-based processes.

#### V. SUMMARY AND CONCLUSIONS

For any ASD process, it is desirable to deposit as much material as possible in the desired growth region before substantial unwanted deposition appears in the non-growth region. Many ASD approaches are being studied, but a quantitative description of the extent of selectivity to compare to competing processes is generally not reported. By developing a quantitative model for random nucleation and growth initiation during ALD on nonreceptive surfaces, the work shows that fitting data to the model allows direct comparison of various ASD methods and provides additional insight into mechanisms that produce unwanted deposition. The model described uses a small number of independent input parameters,  $\hat{N}$ ,  $\hat{N}_0$ ,  $v_d$ , and  $\hat{G}$ , and the output can be readily compared to a wide range of ASD experimental results. The mathematical description includes a full integral model and a simplified spread-sheet compatible model that is simple to implement and captures key trends in the full model.

Fitting the model to experimental results typically requires only one or two fit parameters and allows the extent of unwanted deposition to be quantified, for example, in terms of identified selectivity demarcation parameters that can be defined by a user's target or threshold requirements for successful ASD. Fitting the model to data also shows that in some ASD processes, unwanted film growth begins at nucleation sites present on the starting non-growth surface, while in other ASD processes nucleation sites are more likely generated on the non-growth surface during the deposition process.

The article also highlights the limitations of the model in terms of fundamental chemical processes during film nucleation and unwanted ASD growth. Specifically, while the definition of selectivity used here is based on expected differences in surface reaction thermodynamics and kinetics, the selectivity values obtained in the model correlate to kinetic definitions only over a narrow range of conditions (i.e., only during early film growth). The model also includes several assumptions and simplifications that can in principle be modified and improved. For example, the growth rate  $\hat{G}$  is assumed to be uniform in all directions as expected for common ALD. While the model may give insight even when nuclei are nonhemispherical, the model could be adapted to accommodate alternate growth mechanisms, <sup>20</sup> including, for example, formation and transport of spherical nanoparticle nuclei, 12 facet-selective growth, 14 or nuclei size-dependent catalytic effects. 13

The model output plots for selectivity versus desired film thickness,  $S(t_g)$ , are predominantly empirical values for comparison between processes. Likewise, the model parameters  $\hat{N}$  and  $\hat{N}$  do not provide conclusive evidence, but rather describe surface nucleation conditions consistent with observed data. In some cases, the values for  $\hat{N}$  and  $\hat{N}$  may be related to specific physical mechanisms (e.g.,  $\hat{N}$  may be found to correlate with impurity sites present on the starting substrate surface), but in other cases (such as values of  $\hat{N}$  determined after

deposition and wet etching) the model fit parameters may only provide general insights.

Overall, the quantitative model presented here provides a useful starting point to compare ASD results across the research community, as well as a means to use common experimental tools to gain insight into possible elementary atomic-scale reaction mechanisms that proceed during film growth initiation and nucleation during ALD and related processes. The successful demonstration of the model fit to several distinctly different published ASD data sets provides confidence that the model can be applied broadly to help understand new ASD results and future ASD processes.

#### **ACKNOWLEDGMENTS**

The author acknowledges support for this work from the U.S. National Science Foundation (Award No. 1704151) and from the Semiconductor Research Corporation (Task No. 2401.001). The author also thanks Ian Woodward for his artwork preparing the images in Fig. 1.

- <sup>1</sup>J. O. Carlsson, Vacuum **41**, 1077 (1990).
- <sup>2</sup>J. O. Carlsson, Crit. Rev. Solid State Mater. Sci. 16, 161 (1990).
- <sup>3</sup>J.-O. Carlsson and M. Boman, J. Vac. Sci. Technol. A **3**, 2298 (1985).
- <sup>4</sup>W. L. Gladfelter, Chem. Mater. **5**, 1372 (1993).
- <sup>5</sup>R. Clark, K. Tapily, K.-H. Yu, T. Hakamata, S. Consiglio, D. O'Meara, C. Wajda, J. Smith, and G. Leusink, APL Mater. 6, 058203 (2018).
- <sup>6</sup>M. A. Alam and M. L. Green, J. Appl. Phys. **94**, 3403 (2003).

- <sup>7</sup>R. L. Puurunen *et al.*, J. Appl. Phys. **96**, 4878 (2004).
- <sup>8</sup>O. Nilsen, C. E. Mohn, A. Kjekshus, and H. Fjellvåg, J. Appl. Phys. **102**, 1 (2007).
- <sup>9</sup>R. Vallat, R. Gassilloud, B. Eychenne, and C. Vallée, J. Vac. Sci. Technol. A **35**, 01B104 (2017).
- <sup>10</sup>F. S. Minaye Hashemi, C. Prasittichai, and S. F. Bent, ACS Nano 9, 8710 (2015).
- <sup>11</sup>A. Mameli, M. J. M. Merkx, B. Karasulu, F. Roozeboom, W. E. M. M. Kessels, and A. J. M. Mackus, ACS Nano 11, 9303 (2017).
- <sup>12</sup>F. Grillo, H. Van Bui, J. A. Moulijn, M. T. Kreutzer, and J. R. van Ommen, J. Phys. Chem. Lett. 8, 975 (2017).
- <sup>13</sup>J. Soethoudt, F. Grillo, E. A. Marques, J. R. van Ommen, Y. Tomczak, L. Nyns, S. Van Elshocht, and A. Delabie, Adv. Mater. Interfaces 5, 1800870 (2018).
- <sup>14</sup>K. Cao, J. Cai, X. Liu, and R. Chen, J. Vac. Sci. Technol. A 36, 010801 (2018).
- <sup>15</sup>J. R. Creighton, J. Electrochem. Soc. **136**, 271 (1989).
- <sup>16</sup>P. C. Lemaire, M. King, and G. N. Parsons, J. Chem. Phys. **146**, 052811 (2017).
- <sup>17</sup>C. J. Mogab, J. Electrochem. Soc. **124**, 1262 (1977).
- <sup>18</sup>J. B. Rawlings and J. G. Eckerdt, *Chemical Reactor Analysis and Design Fundamentals*, 2nd ed. (Knob Hill Publishing, Madison, WI, 2013).
- <sup>19</sup>M. Avrami, J. Chem. Phys. **8**, 212 (1940).
- <sup>20</sup>M. Fanfoni and M. Tomellini, Nuovo Cim. D **20**, 1171 (1998).
- <sup>21</sup>M. J. Starink, J. Mater. Sci. **36**, 4433 (2001).
- <sup>22</sup>J. Malek, Thermochim. Acta 355, 239 (2000).
- <sup>23</sup>J. Kwon, T. Yoon, K. Kim, S. Min, J. Appl. Phys. **93**, 3270 (2003).
- <sup>24</sup>H. B. R. Lee, M. N. Mullings, X. Jiang, B. M. Clemens, and S. F. Bent, Chem. Mater. 24, 4051 (2012).
- <sup>25</sup>E. Stevens, Y. Tomczak, B. T. Chan, E. Altamirano Sanchez, G. N. Parsons, and A. Delabie, Chem. Mater. 30, 3223 (2018).
- <sup>26</sup>See supplementary material at https://doi.org/10.1116/1.5054285 for Matlab software code for the nucleation model and brief instructions for implementation.

## A Functional Model for Analysis of ALD Nucleation and Quantification of Area-Selective Deposition

Gregory N. Parsons
Dept. of Chemical and Biomolecular Engineering
North Carolina State University
Raleigh NC 27695

### **Nucleation Model Code**

The code below was written in Matlab, version R2017a. To use the code, all of the lines below can be cut and pasted into a Matlab editor window. The user can the save it, then select "Run" to begin the simulation.

As written, the code specifies input model parameters to be:  $\dot{G} = 0.052 \, \mathrm{nm} \, \mathrm{cyc}^{-1}$ ,  $\hat{N} = 0.01 \, nm^{-2}$ ;  $\dot{N}_0 = 0 \, nm^{-2} cyc^{-1}$ ;  $v_d = 0 \, \mathrm{cyc}$  and  $n = 200 \, \mathrm{cyc}$ , corresponding to the fits shown in Figure 5 a, b and d in the accompanying article. The code also generates a solution matrix called "V", containing the generated fit data and other values, as described in the code comments. A user can adjust the input parameters to any desired values by changing the numbers in the first few lines of the code. A relatively simple modification of the code in the plotting section allows a user's data to be plotted simultaneously with the model output.

```
%% Nucleation and Selectivity Model
% Copyright, Gregory Parsons, 2018
% Code generated by Gregory Parsons August 29, 2018
% Matlab version R2017a
%% Input model parameter values
gdot = .052; % ALD growth per cycle (nm/cycle) on desired growth surface
nhat = 0.01; % density of nucleation sites (per nm^2) on non-growth surface
              % nuclei generation rate (per nm^2 per cycle)
ndot0 = 0;
              % nuclei generation rate incubation cycles (cycles)
td = 0;
ncycles = 200; % number of cycles we want to solve over
%% Set initial values of variables:
AextNdot = 0;
AextNdoth = 0;
AextNhat = 0;
AextNhath = 0;
dAextNdot = 0;
dAextNdoth = 0;
rmax = ncycles+1;
                  % number of rows that we will have in our solution matrix
A0=1;
                    % substrate surface area = 1
%% Calculated results will be put into a solution matrix called V:
   V column 1 = row number
   V column 2 = ALD cycle number (row 2 = cycle 1)
   V column 3 = Calculated thickness on desired growth surface
   V column 4 = Calculated thickness on non-growth surface - full integral.
   V column 5 = Selectivity - from full integral
   V column 6 = Surface film coverage fraction, Af/A0 - from full integral
  V column 7 = Calculated thickness on non-growth surface - estimate
  V column 8 = Selectivity - estimate
   V column 9 Not used
   V column 10 = Number of nuclei - full model
%% Fill in initial values of solution matrix
% Create V matrix with zeros in each cell
V = zeros(rmax, 10);
% We set some values on row 1 (i.e. starting values before ALD starts):
     V(1,1) = 1 ; % Row number
      V(1,5) = 1; % Selectivity - correct integral
      V(1,8) = 1 ; % Selectivity - estimate
     V(1,10) = nhat;
%% Solve for thickness on desired growth area at cycle n
for n = 1: 1 : ncycles
    응응
    r=n+1;
    % Start at cycle #1 (row #2) and do this routine for t = 1 to ncycles.
     V(r,1) = r; % row
      V(r,2) = n; % cycle number r=1, t=0
      V(r,3) = gdot.*n; % thickness on 1
end
```

```
%% Find the fractional surface coverage in non-growth area at cycle n
for n = 1: 1 : ncycles
    r=n+1;
    AextNhat = A0.*pi.*(qdot.*n).^2.*nhat;
    AextNdot = 0;
     for eta = 0: 1: n
           % Parsons notebook Aug 6 p 159
           if td == 0
            dAextNdot = A0.*ndot0.*pi.*(qdot.*(n-eta)).^2;
           else
            dAextNdot = A0.*ndot0.*exp(-td/(n-eta)).*pi.*(qdot.*(n-eta)).^2;
           % Parsons notebook, Aug 6, 2018, page 159
           AextNdot = AextNdot + dAextNdot;
      end % go to next eta
    % Use the Avrami equation to calculate the fractional surface coverage
   V(r,6) = 1 - \exp(-(AextNhat + AextNdot)); % Af/A0
    %% Nucleation site density calculation
    % Parsons' notebook page 133, July 20, 2018.
   V(r,10) = V(r-1,10) + (ndot0.*exp(-td/n).*(1-V(r,6)));
end % go to next n
%% Approximate film thickness and selectivity
for n = 1: 1: ncycles
    r = n+1;
    V(r,7) = V(r-1,7)+V(r,6).*(2-V(r,6)).*gdot; % thickness - estimate
    V(r,8) = (V(r,3)-V(r,7))./(V(r,3)+V(r,7)); %Selectivity - estimate
end
%% Full integration for thickness and selectivity:
for n = 1: 1: ncycles
    r = n+1;
    for stp = 0 : 1 : n
     AextNhath = A0.*pi.*((gdot.*n)^2 - (gdot*stp)^2)*nhat;
     AextNdoth = 0;
      for eta = 0:1:n
        if ((qdot*(n-eta))^2 - (qdot*stp)^2) >= 0 && td == 0
        dAextNdoth = A0*ndot0*pi.*((gdot*(n-eta))^2 - (gdot*stp)^2);
        elseif ((gdot*(n-eta))^2 - (gdot*stp)^2) >= 0
        dAextNdoth = A0*ndot0*exp(-td/(n-eta))*pi*((gdot*(n-eta))^2-(gdot*stp)^2);
        else
        end
         AextNdoth = AextNdoth + dAextNdoth;
        end % next eta
        % Use the Avrami equation to calculate the fractional surface
        % coverage on the non-growth surface at height = stp. This area
        % times the growth rate is the volume at height (stp*gdot)
        V(r,4) = V(r,4) + (1 - exp(-(AextNhath + AextNdoth))).*gdot;
    end % go to next stp (h = stp*dgot)
    V(r,5) = (V(r,3)-V(r,4))./(V(r,3)+V(r,4)); % Selectivity - full integral
end % go to next n
```

```
%% Find t(S=0.9) and S(t=10nm)
fnd90 = find(V(:,5) > 0.90,1,'last');
% change 0.9 to 0.99 to find t(S=0.99)
fnd10 = find(V(:,3) > 10,1);
tS90 = V(fnd90, 3); % t(S=0.9)
S10nm = V(fnd10, 5); % S(t=10nm)
%% Plotting section
subplot(1,3,1)
set(qcf, 'Units', 'Normalized', 'OuterPosition', [0.1, 0.3, 0.8, 0.5]);
plot (V(:,2),V(:,6),'r','linewidth', 1.5) % surface coverage%
xlabel('ALD Cycles') % x-axis label
ylabel('Surface Coverage') % y-axis label
subplot(1,3,2)
plot (V(:,2),V(:,3),'k','linewidth', 1.5) % thickness on 1
xlabel('ALD Cycles') % x-axis label
ylabel('Thickness (nm)') % y-axis label
hold on
plot (V(:,2),V(:,4),'r','linewidth', 1.5) % thickness on 2 - correct integral
hold on
plot (V(:,2),V(:,7),'b','linewidth', 1.5) % thickness on 2 - estimate
hold on
subplot(1,3,3)
plot (V(:,3),V(:,5),'r','linewidth', 1.5) % selectivity - correct integral
xlabel('Thickness (nm)') % x-axis label
ylabel('Selectivity') % y-axis label
plot (V(:,3),V(:,8),'b','linewidth', 1.5) % selectivity - estimate
hold on
% add points on the plot for t(S=0.9) and S(t=10nm)
plot (V(fnd90,3), V(fnd90,5), 'ko', 'MarkerFaceColor', 'k', 'MarkerSize',5)
hold on
plot (V(fnd10,3),V(fnd10,5),'ko','MarkerFaceColor','k','MarkerSize',5)
```